

Mathematical and Computational Models of the Retina in Health, Development and Disease

Paul A. Roberts^{a,b,1,*}, Eamonn A. Gaffney^c, Philip J. Luthert^d, Alexander J. E. Foss^e, Helen M. Byrne^c

^aMathematical Institute, University of Oxford, Andrew Wiles Building, Radcliffe Observatory Quarter, Woodstock Road, Oxford, OX2 6GG, UK

^bDepartment of Computer Science, University of Oxford, Wolfson Building, Parks Road, Oxford, OX1 3QD, UK

^cWolfson Centre for Mathematical Biology, Mathematical Institute, University of Oxford, Andrew Wiles Building, Radcliffe Observatory Quarter, Woodstock Road, Oxford, OX2 6GG, UK

^dInstitute of Ophthalmology, University College London, 11-43 Bath Street, London, EC1V 9EL, UK

^eQueen's Medical Centre, Department of Ophthalmology, Derby Road, Nottingham, Nottinghamshire, NG7 2UH, UK

Abstract

The retina confers upon us the gift of vision, enabling us to perceive the world in a manner unparalleled by any other tissue. Experimental and clinical studies have provided great insight into the physiology and biochemistry of the retina; however, there are questions which cannot be answered using these methods alone. Mathematical and computational techniques can provide complementary insight into this inherently complex and nonlinear system. They allow us to characterise and predict the behaviour of the retina, as well as to test hypotheses which are experimentally intractable. In this review, we survey some of the key theoretical models of the retina in the healthy, developmental and diseased states. The main insights derived from each of these modelling studies are highlighted, as are model predictions which have yet to be tested, and data which need to be gathered to inform future modelling work. Possible directions for future research are also discussed.

Whilst the present modelling studies have achieved great success in unravelling the workings of the retina, they have yet to achieve their full potential. For this to happen, greater involvement with the modelling community is required, and stronger collaborations forged between experimentalists, clinicians and theoreticians. It is hoped that, in addition to bringing the fruits of current modelling studies to the attention of the ophthalmological community, this review will encourage many such future collaborations.

Keywords: Oxygen, Neuroglobin, Photoreceptors, Angiogenesis, Retinitis Pigmentosa, Choroidal Neovascularisation.

1	Contents	12	5 Disease	14
2	1 Introduction	13	5.1 Retinitis Pigmentosa	14
3	2 Mathematical and Computational Modelling	14	5.1.1 The Trophic Factor Hypothesis	14
4	3 Health	15	5.1.2 The Toxic Substance Hypothesis	15
5	3.1 Retinal Oxygen Distribution	16	5.1.3 The Oxygen Toxicity Hypothesis	16
6	3.2 Neuroglobin	17	5.2 Choroidal Neovascularisation	19
7	3.3 Choriocapillaris	18	6 Perspective and Future Directions	21
8	3.4 Photoreceptors	19	1. Introduction	
9	4 Development	20	The retina is a complex and highly structured tissue. Cover-	
10	4.1 Retinal Angiogenesis	21	ing the inner surface of the back of the eye, it captures incident	
11	4.2 Retinal Mosaic Formation and Retinogenesis	22	light, generating electrochemical signals, which, after some ini-	
		23	tial processing, are transmitted to the brain via the optic nerve,	
		24	giving rise to visual perception. As such, it is arguably the most	
		25	important means by which we gain information about the world	
		26	around us.	
		27	The last two decades have seen a rapid increase in the use	
		28	of mathematical and computational modelling techniques in the	
		29	biological sciences, due, in part, to an increase in computational	
		30	resources. These methods have been applied to a plethora of	
		31	systems, across a range of spatial and temporal scales, from the	

*Corresponding author

Email addresses: p.a.roberts@univ.oxon.org (Paul A. Roberts), gaffney@maths.ox.ac.uk (Eamonn A. Gaffney), p.luthert@ucl.ac.uk (Philip J. Luthert), alexander.foss@nottingham.ac.uk (Alexander J. E. Foss), helen.byrne@maths.ox.ac.uk (Helen M. Byrne)

¹Present address: School of Mathematics, University of Birmingham, Edgbaston Campus, Birmingham, B15 2TT, UK

²ODE: ordinary differential equation, PDE: partial differential equation, Rd-CVF: Rod-derived cone viability factor, MSS: mutant steady-state.

ecological, through to the molecular scale and from the evolutionary timescale to the rapid firing of neurons [59, 60, 87, 88]. As a consequence, a wealth of insights have been generated that would have been difficult, and in many cases impossible, to achieve through the use of experimental or diagnostic techniques alone.

The revolution in mathematical and computational biology has not left eye and retinal research untouched, with a host of models exploring the biomechanics of the eye [14, 38, 96], glaucoma, flow within the aqueous and vitreous humours [7, 102, 108] and the dynamics of the tear film [11, 12, 61]. A number of models of the retina have also been developed, though modelling in this area has been less extensive than that devoted to other aspects of the eye. The purpose of this review is to highlight insights that have been gained from theoretical studies of the retina and to stimulate further modelling work and theoretical/experimental collaborations in this area.

Whilst experimental and clinical studies can reveal many of the physiological and biochemical details of the retina, there are limits to the questions that can be answered using these techniques alone. Mathematical and computational modelling allows us to extend these horizons in at least three ways. Firstly, it allows us to understand and predict the behaviour of systems which involve *nonlinearities*, such as those generated by feedback mechanisms in biochemical reaction networks, or those which arise in the mechanics of fluid flow (see Sections 3.3 and 5.1.1 for examples). The sensitivity of the system to alterations in each component can be tested, and the range of qualitative behaviours that it may exhibit, together with the conditions under which they are realised, may be determined. Thus, by placing a problem in a modelling framework, we gain insight into why a system behaves as it does, when it does. Secondly, modelling allows us to *isolate mechanisms*, or manipulate a system, in ways that may not be possible experimentally. An example of this is discussed in Section 5.1.3, where oxygen toxicity is assumed to be the only cause of photoreceptor death in retinitis pigmentosa. Lastly, modelling allows examination of a *wider range of scenarios* than would be possible experimentally, since *in silico* (computer simulation) studies are not subject to the same financial and time constraints as those performed *in vivo* or *in vitro*. This is seen clearly in Section 5.2, where the effects of a range of inter-cell adhesivities on the progression of choroidal neovascularisation are investigated.

How, then, can mathematical and computational models be integrated with experimental and clinical studies? In Figure 1, we sketch out the basic contours of this relationship. We begin with the system to be modelled and all that is known about it. Upon this foundation, and guided by a set of well-defined questions, we build our theoretical model. In so doing, we make a series of *simplifying assumptions*, including only those features of the system which are thought to be significant and of relevance to the questions under consideration. The nature of the system and the questions we bring to it will also influence the type of model we develop (see Section 2 for a discussion of model types). Having formulated our model, we use *mathematical analysis* and/or *computational simulations* to derive solutions. Comparing these solutions with our current knowl-

edge, we find that the model is either successful or unsuccessful in replicating its known behaviours. If unsuccessful, the model is revised and fresh solutions generated; if successful, the model is then used to make *predictions* that lie outside our knowledge domain, in an attempt to answer our earlier questions. These predictions may then be tested experimentally. If the experiments match with model predictions then we may have some confidence that we have answered our questions, whilst if they do not, then we must revise our model and compare it once more with known system behaviour, returning to an earlier point in the *modelling/experiment cycle*. Insight is gained at two main stages during this process. Firstly, insight is gained at the *benchmarking* stage (see Figure 1), which reveals whether or not the mechanisms included in the model are sufficient to replicate known behaviour. Secondly, insight is gained when experimental/clinical studies confirm model predictions (see Figure 1).

The above description does not perfectly represent the approach taken in all of the modelling studies presented below, but it serves as a basic framework. Depending upon what data are available, it may be difficult to benchmark the model and many modelling predictions are left to gather dust without experimental confirmation. It is important to note that it is unhelpful to simply characterise models as either right or wrong, since any model is a *simplified representation of reality* and hence always, in some sense, wrong. A more fitting way of classifying them would be as *useful* or *useless*. A model is useful if it replicates current data enabling us to make predictions, or if it fails to replicate current data, but in such a way as helps us to identify missing or unwarranted features of the model. It is useless if it fails in both of these respects.

The process of constructing a mathematical model is itself informative, as it forces us to think about the biological system in a new way, formalising and consolidating the questions being addressed. Whilst the primary motivation for modelling arises from questions raised by experimentalists, it is often not until this stage, or those which follow, that many of the questions that we wish to pose to the model occur to us; insights emerging unexpectedly and unlooked for, as a result of this new way of thinking.

The remainder of this paper is structured as follows. In Section 2, we review some of the mathematical and computational techniques used in the modelling studies discussed in this paper. In Sections 3–5, we examine a set of retinal models from across a range of *healthy*, *developmental* and *diseased* states. In each case, we describe the problem, the model and the results generated, comparing them with experimental and clinical data. Testable model predictions are highlighted, as are areas where more experimental data are needed to inform future modelling studies. Lastly, in Section 6, we summarise the state of the field and suggest directions for future research.

2. Mathematical and Computational Modelling

In seeking to mathematically describe a biological system, we must choose between a range of *model types*. Whilst there may be no unique best model, our selection will be guided by

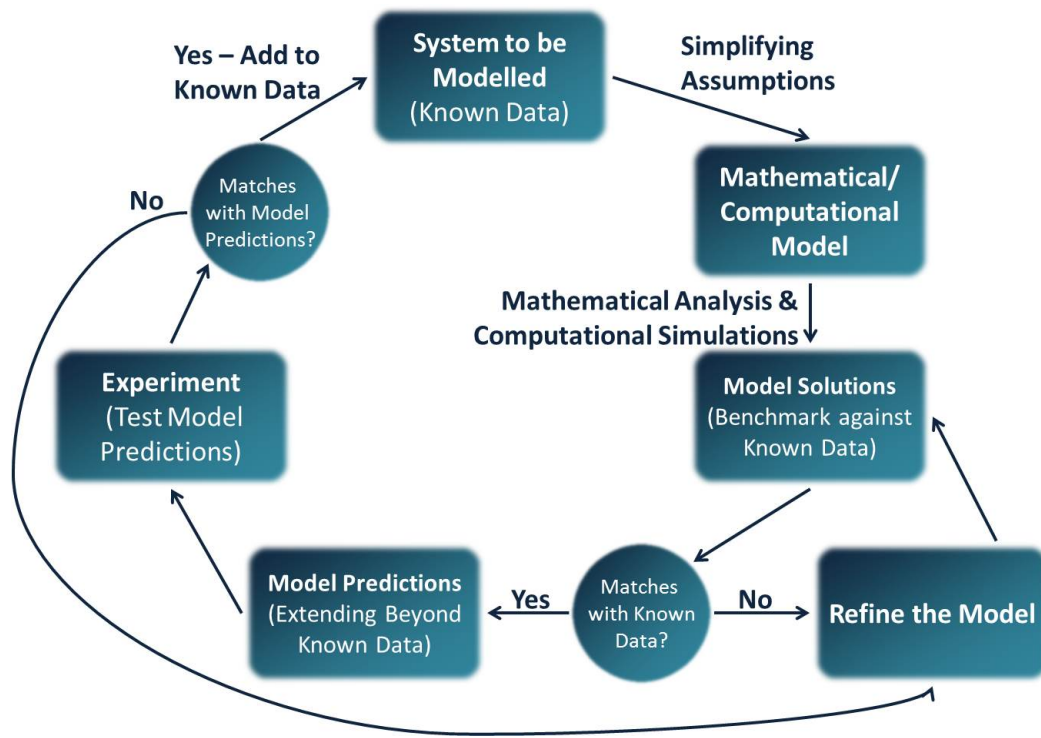


Figure 1: The experiment/modelling cycle. Mathematical and computational models are derived to answer questions arising from what is known about the biological system. Model solutions are then compared with known data and refinements to the model are made where necessary. Once successfully benchmarked, the model is used to make predictions which may then be tested experimentally. Further model refinements may be necessary at this stage. Agreement between modelling predictions and experimental results gives us confidence that we have gained reliable new knowledge about the system.

144 the form of the system and the questions which we aim to address. Each type of model has *advantages* and *disadvantages* and will involve making simplifying assumptions. Table 1 provides an overview of the available options. In what follows, we summarise some key model types. This is not intended as a comprehensive overview; rather, it is tailored to the modelling studies that are presented in the remainder of this paper.

151 *Phenomenological models* are designed simply to fit with experimental data, and neglect the underlying mechanisms that gave rise to them, whereas *mechanistic models* are designed to describe the underlying processes, such that, if they are accurate, behaviour consistent with the data will emerge naturally from the system. In practice, no model is fully mechanistic, its components reducing at some level to the phenomenological. The models presented below are all mechanistic.

159 As the title of this paper indicates, we distinguish between *mathematical* and *computational models*, though we note that this is not a sharp distinction, there being areas of overlap between the two model types. Broadly speaking, computational models require simulation to reveal their behaviours, whereas the behaviour of mathematical models can be revealed by the application of analytical techniques (see the discussion of analytical techniques below). Typically, mathematical models comprise only a few equations (the trophic factor model in Section 5.1.1 contains no more than 4 governing equations), whilst computational models involve either a large system of equations and/or an algorithmic component (see, for example, the

choroidal neovascularisation model in Section 5.2, where the movement of cells is described algorithmically). Thus, computational models tend to be more comprehensive, whilst mathematical models allow for a more intuitive understanding of the system.

If a system is homogeneous or spatial variation is unimportant, then a *well-mixed*, spatially-independent model may be used (this is the case in the trophic factor model in Section 5.1.1, where the spatial distribution of rods and cones is ignored), the focus being the temporal evolution of the system. If, however, spatial structure is important, then either a *compartmental* or *spatial model* is required. Compartmental models decompose the system into a set of spatially homogeneous compartments, with terms to describe how material may be exchanged between them (for instance, the toxic substance model in Section 5.1.2 identifies each photoreceptor with an individual compartment, governed by its own equation), whilst fully-spatial models allow for spatial heterogeneity within the same compartment (see, for example, the models of retinal oxygen distribution in Section 3.1, where the oxygen concentration is allowed to vary across each model layer).

If we are interested simply in the resting state of a system, then a *steady-state model* (in which the system does not change with respect to time) can be used, whereas, if the dynamic behaviour of the system is important, then a *time-dependent model* is needed (where the system evolves over time). For example, the oxygen distribution models in Section 3.1 are of the steady-

Table 1: Model types. Contrasting types of models are described and their advantages and disadvantages noted.

Model Type	Description/Assumptions	Advantages	Disadvantages
Phenomenological vs Mechanistic	Designed to match the experimental data Designed to capture the underlying processes	Close fit to data Insight generated	Little insight Loose fit to data
Mathematical vs Computational	Fully described by a set of mathematical equations Relatively simple Require simulation to reveal their behaviour Typically complex	Analytically tractable and generally not computationally expensive Detailed	Lacks detail Not analytically tractable and often computationally expensive
Well-mixed vs Compartmental/Spatial	Spatial structure and effects are neglected Spatial distributions and compartmentalisation are accounted for	More tractable Spatial effects captured	Spatial effects neglected Less tractable
Steady-state vs Time-dependent	The system does not vary in time The system may evolve over time	More tractable Dynamics captured	Dynamics lost Less tractable
Continuous vs Discrete	The system is continuous in space and time The system moves between discrete states in space and time	More analytically tractable and generally not computationally expensive Many details captured	Details lost Less analytically tractable and often computationally expensive
Deterministic vs Stochastic	Simulations run under the same conditions produce the same solution The model contains a probabilistic component Simulations run under the same conditions produce different solutions	Substantial analytical insight Accounts for noise	Does not account for noise Little analytical insight

state form, oxygen profiles being assumed to change very little under normal conditions, whilst the photoreceptor models in Section 3.4 are time-dependent, so that they can capture time variation in outer segment length.

If the objects being modelled (e.g. cells or molecules) are numerous and small in relation to the spatial domain in which the model is being solved, then cell populations may be treated as continuous densities and chemicals as concentrations (see, for example, the oxygen toxicity models in Section 5.1.3, where photoreceptors are treated as densities and oxygen as concentration). *Continuum models* may be analytically tractable, allowing us to derive analytical solutions (see below) and hence predict how a system will behave under different conditions. If the above assumptions do not hold, then a discrete model is appropriate. *Discrete models* may incorporate more detail than continuous models, but are more computationally expensive, with computational costs increasing dramatically as the number of objects is increased. For example, the retinal an-

giogenesis model in Section 4.1 treats blood vessels as discrete entities, allowing it to capture their intricate spatial structure.

Lastly, a distinction may be made between *deterministic* and *stochastic models*. Deterministic model simulations run under the same conditions always produce the same solution (see, for example, the choriocapillaris blood flow models in Section 3.3), whilst stochastic models incorporate a probabilistic element, capturing the ‘noise’ of a biological system, as a result of which, each simulation is different (an example being the stochastic apoptosis of photoreceptors in the toxic factor model in Section 5.1.2, see de Vries et al. 34 for a description of stochastic techniques). In recent years, continuous-deterministic and discrete-stochastic models have been combined in what are known as *hybrid models* (as in the retinal angiogenesis model in Section 4.1).

Continuous-deterministic models are typically described in terms of *ordinary differential equations* (ODEs) and *partial differential equations* (PDEs). ODEs are used in well-mixed and

234 compartmental models, where they describe the evolution of the
 235 system with time (e.g. Sections 5.1.1 and 5.1.2), and are also
 236 used in one-dimensional (1D) steady-state models (e.g. Section
 237 3.1). PDEs are used for dynamic spatial models in 1D, 2D or
 238 3D and for steady-state models in 2D or 3D (e.g. Section 5.1.3).

239 In defining a problem, a number of factors must be taken
 240 into consideration. Firstly, where the model is spatial, we must
 241 describe the (1D/2D/3D) *geometry* of the domain on which the
 242 problem is to be solved. *Governing equations* must be imposed
 243 in the domain, and combined with *initial conditions* (to describe
 244 the state of the system at time $t = 0$) and *boundary conditions*
 245 (to describe the behaviour of the problem at the domain bound-
 246 aries). Lastly, values must be assigned to the *model parameters*,
 247 using experimentally measured data where possible.

248 Having defined a model, we may investigate its behaviour.
 249 Typically, the models which arise from biological problems do
 250 not admit explicit *analytical solutions*. That is, we cannot find
 251 algebraic expressions for the dependent variables (e.g. cell den-
 252 sity or chemical concentration) in terms of the independent vari-
 253 ables (space and time) together with the model parameters. In-
 254 stead, we must proceed in one or both of the following two
 255 ways. Firstly, we may solve our equations *numerically*. For
 256 ODE and PDE models, this may involve methods such as the
 257 finite difference method (or method of lines) and the finite ele-
 258 ment method, which involve discretising our equations in space
 259 and time [see 85, 111, for details]. Secondly, we may use *an-*
 260 *alytical methods* to systematically reduce the governing equa-
 261 tions to a simpler form. Commonly used analytical methods
 262 include asymptotic analysis, which reduces the system to its
 263 dominant components, and steady-state and bifurcation anal-
 264 yses, which allow us to determine the stability properties of
 265 the system i.e. whether the system behaviour is insensitive to
 266 small perturbations, and how such responses vary as paramet-
 267 ers are altered [see 53, 110, for details]. Often, a combination
 268 of numerical and analytical techniques is used to provide a more
 269 complete picture, consistent results giving an added degree of
 270 confidence in the model and solution methods. Lastly, since the
 271 parameter values in our models are frequently estimated and of-
 272 ten subject to variability, *sensitivity analyses* may be performed
 273 to determine the effect of parameter variation on model predic-
 274 tions.

275 3. Health

276 3.1. Retinal Oxygen Distribution

277 The mammalian retina has a multilayered structure consist-
 278 ing of numerous cell types (see Figure 2). The *outer retina* con-
 279 tains two cellular layers: the *retinal pigment epithelium* (RPE)
 280 and the light-detecting *photoreceptors*, which can be charac-
 281 terised as either *rods* or *cones*, whilst the *inner retina* also con-
 282 tains two cellular layers: a layer consisting of bipolar, horizon-
 283 tal, amacrine and Müller cells, and the ganglion cell layer. The
 284 inner layers are responsible for preprocessing of visual informa-
 285 tion and its subsequent transmission to the brain, via the optic
 286 nerve and are separated from the vitreous humour by the *inner*
 287 *limiting membrane* (ILM).

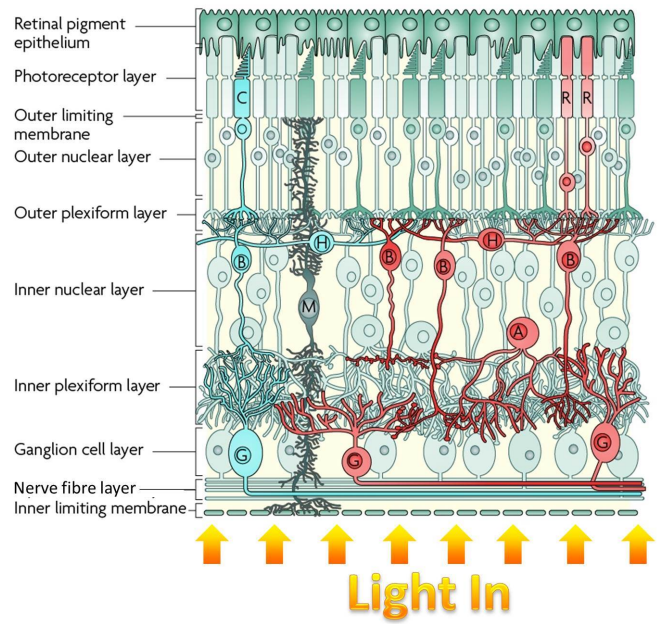


Figure 2: Diagram of the human retina. The retina is composed of four cellular layers: the outer retina contains the retinal pigment epithelium and photoreceptor layers, whilst the inner retina contains bipolar/horizontal/amacrine/Müller glial cell and ganglion cell layers. The diagram is oriented such that the top lies outermost and the bottom innermost in the eye. R: rod photoreceptor. C: cone photoreceptor. H: horizontal cell. B: bipolar cell. M: Müller glial cell. A: amacrine cell. G: ganglion cell. Figure reproduced, with permission and modifications, from Swaroop et al. [112], where modifications are reproduced, with permission, from Roberts et al. [93].

The retina consumes oxygen at a higher rate than most other tissues in the mammalian body [4, 5, 118, 126]. To meet this need, it is equipped with an extensive vasculature. The outer retina is supplied mainly by the *choroid*, which lies outward from the retina, separated from the RPE by Bruch's Membrane, whilst the inner retina is supplied by *retinal capillary layers*, of which there are typically two, one deep and the other superficial. The magnitude of oxygen supply and demand render the retina vulnerable to both *hypoxia* (oxygen deprivation) and *hyperoxia* (toxically high oxygen levels). Therefore, it is of interest to understand how the retina is maintained in *normoxia* (favourable oxygen levels) in health, and how and why the oxygen profile changes in disease states such as vascular occlusive diseases, diabetic retinopathy, retinopathy of prematurity and retinitis pigmentosa [118].

Oxygen sensitive microelectrodes have been used to measure the partial pressure of oxygen across the width of the retina, from the ILM to the choroid, in a variety of mammals and under a range of conditions [see 118, 126, 128, 129, for reviews]. Whilst it is helpful to determine the oxygen profile (comparisons between profiles providing insight even in the absence of a model), the measurement does not, by itself, help us to understand why the profile takes the shape that it does. In order to explain the profile, we must determine the rates of oxygen supply and demand, and how these vary across the retina.

A number of mathematical models have been developed to

314 describe and explain retinal oxygen measurements. These mod-368
 315 els typically assume that the system is at *steady-state* (i.e. not369
 316 varying with time) and are posed on a *one-dimensional Carte*-370
 317 *sian geometry*, across the width of the retina, perpendicular to371
 318 the wall of the eye. Using a Cartesian geometry, rather than372
 319 a spherical geometry, is justified, since the width of the retina373
 320 is much smaller than the radius of curvature of the eye. It is374
 321 further typically assumed that the rate of oxygen consumption375
 322 is *piecewise constant* across the retina. As such, the retina is376
 323 decomposed into a series of n *discrete intervals* $0 < x < L_1$,377
 324 $L_1 < x < L_2, \dots, L_{n-1} < x < L_n$ (see Figure 3), where x is the378
 325 distance from the *choriocapillaris* (CC, the innermost layer of379
 326 the choroid). Within each interval, the rate of oxygen uptake is380
 327 given by a constant, Q_i (for $i = 1, \dots, n$). Therefore, invoking381
 328 Fick's second law, these models reduce to the following ODEs:382

$$329 \quad D \frac{d^2 c}{dx^2} = Q_i, \quad \text{for } i = 1, \dots, n, \quad (1) \quad 383$$

330 where $c(x)$ is the oxygen concentration and D is the diffusivity386
 331 of oxygen. These equations may be solved to give387

$$332 \quad c(x) = \frac{Q_i x^2}{2D} + A_i x + B_i, \quad \text{for } i = 1, \dots, n, \quad (2) \quad 388$$

333 where the constants of integration, A_i and B_i ($i = 1, \dots, n$), are389
 334 determined by imposing boundary conditions at all external and392
 335 internal boundaries. As such, the profiles are *piecewise linear*393
 336 (for $Q_i = 0$) and *quadratic* (for $Q_i \neq 0$), where $Q_i > 0$ indicates394
 337 a net *uptake* and $Q_i < 0$ a net *supply* of oxygen.395

338 To date, most models have restricted their attention to the396
 339 avascular outer retina [35, 52, 68]. Since the inner retinas of397
 340 most mammals are penetrated by deep and superficial retinal398
 341 capillary beds, it is not possible, using these models, to distin-399
 342 guish between oxygen supply and consumption in this region.400
 343 Two resolutions to this problem have typically been considered:401
 344 use animals with avascular inner retinas such as the rabbit or402
 345 guinea pig [32, 107], or occlude the retinal capillaries [10, 35].403
 346 In this way, the models can be extended to describe the entire404
 347 retina, and the oxygen consumption of each layer determined.405
 348 Other authors include the inner retina without occlusion, but
 349 cannot distinguish between supply and uptake [33].406

350 In many theoretical studies, the number of model layers is
 351 varied to determine the minimum number required to obtain a
 352 good fit to experimental data, the number being increased until
 353 the improvement in fit is deemed insignificant, or the model
 354 becomes sensitive to noise in the data [10, 52, 68]. The earliest
 355 such models are those of Dollery et al. [35] who used single
 356 layer models for the outer retina and the whole retina. Later,
 357 Linsenmeier [68] and Stefánsson [107] developed two layer
 358 models for the outer retina and for the inner and outer retina
 359 respectively. This was followed by a three layer model of the
 360 outer retina [52], to which a fourth layer was later added, to en-
 361 compass the inner retina [10]. The most detailed model of this
 362 type to date is that due to Cringle and Yu [33], who decompose
 363 the retina into eight layers. Model layers representing either
 364 entire *cellular layers* (e.g. the ganglion cell layer), or *subcom-*
 365 *partments* within cellular layers (e.g. the photoreceptor inner
 366 segment layer).421

Once the number of model layers has been fixed, the mod-
 els may be fit to the experimental profiles by varying the L_i s
 (except L_n , the total retinal width), Q_i s and oxygen concentra-
 tions on the external boundaries upon which Dirichlet bound-
 ary conditions (at which the oxygen concentration is held at a
 fixed value) have been imposed. In this way, one can determine
 the (net) oxygen consumption in each layer of the retina and
 thereby explain why the profile takes the shape that it does.

This approach has led to some important discoveries. For
 example, it has been shown that the photoreceptor *inner seg-*
ments (ISs) are the dominant oxygen consumers in the outer
 retina, consuming approximately twice as much oxygen under
dark adaptation (DA) as under *light adaptation* (LA) [52, 68].
 Meanwhile, the outer region of the inner plexiform layer (IPL)
 dominates consumption in the inner retina, exceeding that of
 the photoreceptor ISs [33]. Other discoveries include an expla-
 nation for how inner retinal normoxia is maintained when the
 oxygen content of inspired air increases, via increased uptake
 by the outer plexiform layer (OPL) and the outer region of the
 IPL, and how outer retinal *anoxia* (complete oxygen depletion)
 is prevented under DA in the rat, through increased oxygen deli-
 very from the CC and deep retinal capillary layer [33, 127].
 [See 118, 126, 128, 129, for detailed reviews.]

Whilst the above models have proved fruitful, they have two
 key limitations. Firstly, they do not distinguish between uptake
 and supply in the vascular inner retina, and, secondly, they do
 not account for the variation in oxygen uptake with local oxy-
 gen concentration, this effect becoming significant in those re-
 gions where the oxygen profile approaches hypoxic levels.

Roberts et al. [93] have developed a model which addresses
 these limitations (see Figure 3, where layers 6 and 7 are com-
 bined in this case, reducing the model to 7 layers). Uptake
 and supply are distinguished by accounting for the retinal capil-
 lary layers through boundary conditions between model layers,
 whilst the dependence of oxygen uptake upon the local oxygen
 concentration is accounted for by replacing the constant uptake
 term, Q_i , with a *Michaelis-Menten* term, $Q_i c / (\gamma + c)$, so that
 equation (1) becomes

$$D \frac{d^2 c}{dx^2} = \frac{Q_i c}{\gamma + c}, \quad \text{for } i = 1, \dots, 7, \quad (3)$$

where γ , the Michaelis constant, is the oxygen concentration
 at which the oxygen consumption rate is half maximal ($Q_i/2$).
 The model describes the mid-peripheral human retina (with seven
 layers required to account for the spatial variation in oxygen
 consumption and the presence of capillary layers), though it
 could be adapted to model any mammalian retina by adjusting
 the number and arrangement of layers and the boundary condi-
 tions between layers. As with the previous studies, this model
 could also be fitted to experimental profiles. Unlike equation
 (1), equation (3) does not have an analytical solution and so
 must be solved numerically.

Mathematical analysis of Roberts et al.'s model reveals that
 the earlier piecewise linear and quadratic models (equations (1)
 and (2)) are valid, provided the oxygen concentration does not
 approach hypoxic levels, oxygen levels below 1 mmHg being

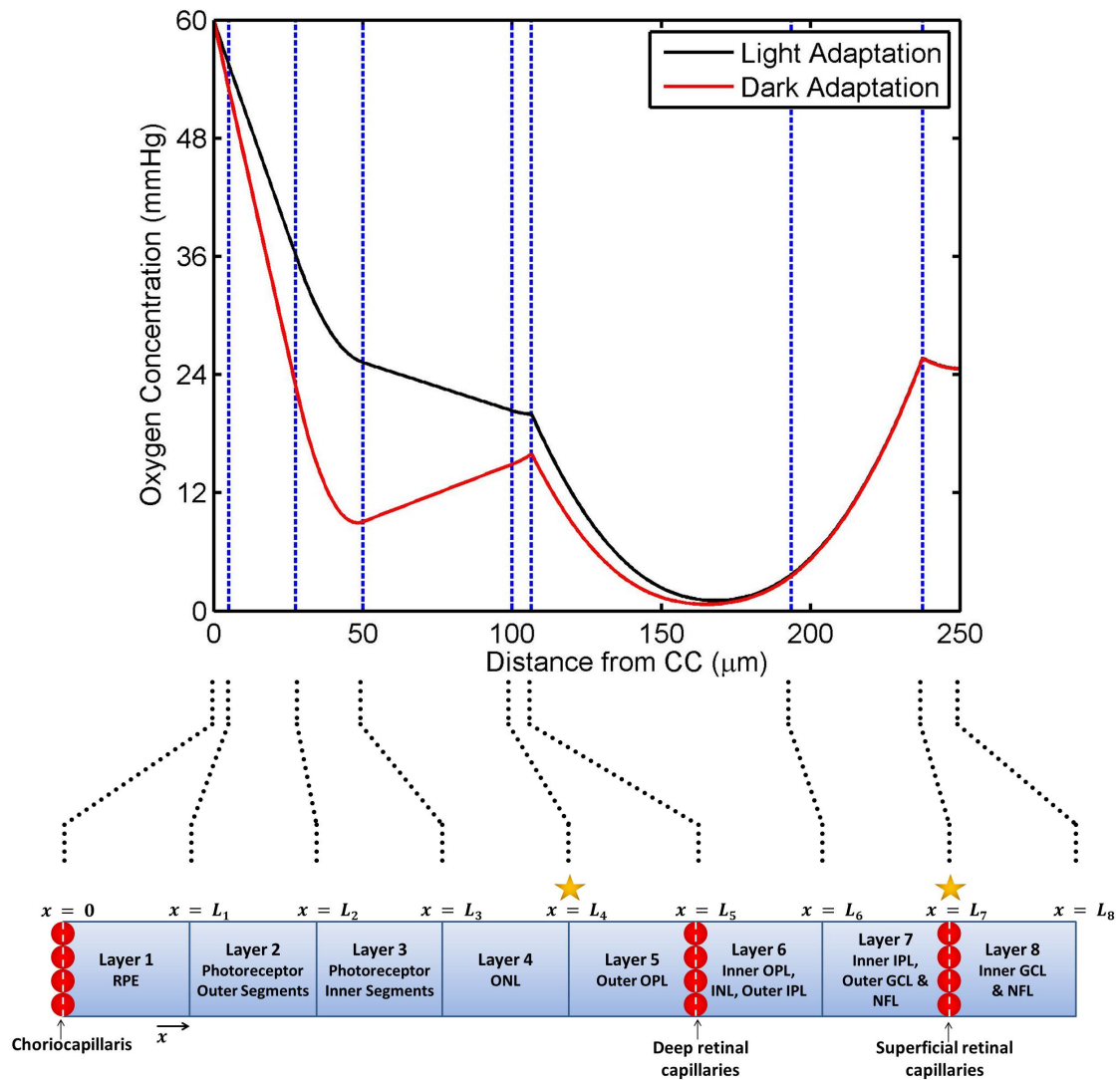


Figure 3: Roberts et al.'s retinal oxygen distribution model. Bottom: diagram to show the model geometry. Oxygen is supplied to the tissue via the CC and retinal capillaries, whilst the net-flux of oxygen at $x = L_8$ is zero. The concentration and flux of oxygen is continuous across all other boundaries. The flux of neuroglobin (Ngb) between layers is zero, except at those boundaries marked with stars, across which the concentration and flux of Ngb is continuous. In the case where Ngb is not included, layers 6 and 7 may be combined, reducing the model to 7 layers. Top: simulation results showing the oxygen distribution in the healthy human retina under LA and DA in the absence of Ngb. The spatial extent of the model layers is depicted by the dashed vertical lines. The oxygen concentration in the outer retina (layers 1–5) and layer 6 is significantly lower under DA, due to the increased rate of oxygen uptake by the photoreceptor ISs. CC: choriocapillaris, RPE: retinal pigment epithelium, ONL: outer nuclear layer, OPL: outer plexiform layer, INL: inner nuclear layer, IPL: inner plexiform layer, GCL: ganglion cell layer, NFL: nerve fibre layer. Figure reproduced, with permission and modifications, from Roberts et al. [93].

422 considered hypoxic [78, 93]. Quadratic approximations are also 433
 423 valid in hypoxic, or near-hypoxic regions; however, the coeffi- 434
 424 cients must be modified as described in Roberts et al. [93]. This 435
 425 analysis therefore places the previous models on a stronger *the*- 436
 426 *oretical foundation*, whilst also enabling them to be extended to 437
 427 account for a broader range of scenarios. 438

428 Whilst Roberts et al.'s model resolves some of the weak- 439
 429 nesses in previous models, it has limitations. In particular, by 440
 430 placing capillary layers along the boundaries between model 441
 431 layers, it assumes that the capillaries lie in a plane. Whilst 442
 432 this is reasonable for the two retinal capillary layers in the mid- 443

periphery of the human retina and in the retinas of many other
 mammals, some capillary layers, such as the additional layers
 found in the peripapillary area of the human retina, are more
 diffuse [23, 64, 81, 90, 104, 113]. In these cases, it would
 be more appropriate to incorporate a distributed oxygen source
 term into those layers that contain capillary beds. Provided the
 capillary surface area, permeability and oxygen concentration
 could be measured, it would still be possible to distinguish be-
 tween uptake and supply.

In addition to considering oxygen levels within the retina,
 modellers have investigated oxygen transport within the *retinal*

444 *vasculature*. In particular, Liu et al. [70] constructed a model of 499
445 the flow distribution and oxygen transport within a 2D retinal 500
446 arterial network. The central retinal arterial geometry was re- 501
447 constructed from an image of the human fundus and the periph- 502
448 eral circulation added using a structured tree model, allowing a 503
449 prediction for the oxygen distribution within a retinal network. 504
450 Further, Ganesan et al. [45, 46] created a network model of the 505
451 murine retinal vasculature, incorporating all three layers (the 506
452 superficial layer, containing veins and arterioles, and the inter- 507
453 mediate and deep capillary networks). The veins and arterioles 508
454 of the superficial layer were modelled directly using data from 509
455 the image analysis of the murine retina, whilst the capillary lay- 510
456 ers were represented using uniformly distributed meshes. This 511
457 model produced a number of interesting further results; for in- 512
458 stance, it was found that the blood *haematocrit* (the ratio of 513
459 red blood cell volume to total blood volume) is smaller close 514
460 to the optic disc and greater toward the periphery. While such 515
461 modelling frameworks do not describe oxygen levels in the sur- 516
462 rounding tissue, it would be feasible to couple vascular oxy- 517
463 gen transport models with tissue oxygenation models to explore 518
464 how retinal vascular disease disrupts oxygen supply. 519

465 Finally, we note that theoretical studies have also consid-
466 ered the *transmural transport* of oxygen to the retina, as well 520
467 as oxygen transport and consumption within the vitreous [see, 521
468 40, 43, 98, for further details]. 522

469 3.2. Neuroglobin 524

470 Given the retina's extensive oxygen demand, any factor which 525
471 contributes to the supply of oxygen could be vital in preventing 526
472 hypoxia. It has been suggested that the protein *neuroglobin* 527
473 (Ngb), which is present in high concentrations in the retina, 528
474 could enhance the retinal oxygen supply [17]. A number of 529
475 lines of evidence indicate such a role, most notably its simi- 530
476 larity in structure and molecular mass to myoglobin; however, 531
477 opinion about its role remains divided [see 13, 15, 16, 39, 89, 532
478 for reviews]. 533

479 In theory, Ngb could enhance the oxygenation of retinal tis- 534
480 sue via two distinct yet related processes, namely *transport* and 535
481 *storage*: Ngb could transport oxygen from regions where it is 536
482 plentiful to others where it is scarce and provide a temporary 537
483 supply of oxygen during periods of decreased supply or in- 538
484 creased uptake. The first scenario (transport) is best considered 539
485 using a steady-state (ODE) model, whilst the second (storage) 540
486 requires a *time-dependent* (PDE) model. 541

487 To date, only two modelling studies have been conducted 542
488 to investigate the oxygen transport and storage properties of 543
489 Ngb. Fago et al. [39] developed a three layer model of the outer 544
490 retina, consisting of a central region that consumes oxygen and 545
491 contains Ngb, and two outer layers that do not consume oxy- 546
492 gen and are devoid of Ngb. The proportion of Ngb molecules 547
493 in their oxygen-bound and unbound states is assumed to be at 548
494 *quasi-steady-state* at all times (that is, the two species are in 549
495 equilibrium). Their results suggest that the concentration of 550
496 Ngb in the middle layer would need to exceed $100\ \mu\text{M}$ for Ngb 551
497 to be effective in storage and to exceed $300\ \mu\text{M}$ to be effective 552
498 in transport. Since they assume that the local Ngb concentration 553
554

could not exceed these values, they conclude that Ngb does not
play a significant role in transport and storage.

Given that the average Ngb concentration across the retina
has been estimated to lie in the range $100\text{--}200\ \mu\text{M}$, Roberts
et al. [93] have argued that, since Ngb is confined to the cy-
tosol of retinal cells and since it is more highly concentrated in
some retinal layers than others, the local cytosolic concentra-
tions in some layers could significantly exceed $200\ \mu\text{M}$. They
constructed an eight layer model, spanning the full width of
the (human) retina and relaxing Fago et al.'s quasi-steady-state
assumption (see Figure 3). The model confirmed that Ngb is
unlikely to play a significant role in oxygen storage, demon-
strating that whilst it will delay a drop in oxygen levels, it will
also delay recovery [92]. However, the model suggests that Ngb
could prevent hypoxia in the ISs and IPL via transport, increas-
ing oxygen uptake by up to $30\text{--}40\%$ in these regions. Further, it
was demonstrated, using a simplified, single layer model, that
the lower *affinity* for oxygen of Ngb than myoglobin may be
advantageous for oxygen transport, contrary to the prevailing
view [15, 16, 39]. Indeed, many of the measured Ngb oxygen
affinities appear to be close to optimal.

523 3.3. Choriocapillaris 524

Zouache et al. [131] have developed a model to describe
the blood flow within the *choriocapillaris* (CC). The CC is the
inner layer of the choroid, responsible for supplying the outer
retina with oxygen and other nutrients, and for removing waste
products. It is subdivided into independent tessellating poly-
gonal units known as *lobules*. These compartments are essen-
tially planar, and are supplied and drained by microvessels, ly-
ing deeper in the choroid, via *inlets* and *outlets*, which feed into
the outer surface of the lobules, perpendicular to their plane
[131]. Blood is supplied at the centre of each lobule by an arte-
riole, and drained at the surrounding vertices by venules. Whilst
these compartments are not physically divided from each other,
neighbouring outlets are connected by *separatrices* (streamlines
which divide the flow into regions with different kinds of mo-
tion) in the blood flow, on which the residence time is long,
forming an effective barrier between adjacent lobules [131].
Lobules are interspersed by avascular *septal pillars*, which stretch
between the inner and outer boundaries, interrupting blood flow.
The pillars are randomly distributed, with a uniform distribution
[131].

Rather than model the entire CC, Zouache et al. [131] con-
sider an individual lobule. The model is further simplified by
decomposing lobules into *triangular prisms*, with the inlet at
one vertex and outlets at the other two (see Figure 4(a)). For
simplicity, the triangle is assumed to be isosceles, the inlet be-
ing separated from the outlets by sides of equal length. The
internal angle at the inlet and the *septae volume fraction* (the
proportion of the domain occupied by septae) are varied to rep-
resent lobules at different geographical locations within the eye.

Since the height of a lobule is much smaller than the width
of the septal pillars, the component of the flow perpendicular
to the inner and outer boundaries can be neglected. Averaging
the fluid velocity across the height of the lobule, the model is
reduced to a *planar* (2D) flow. The flow is further assumed to

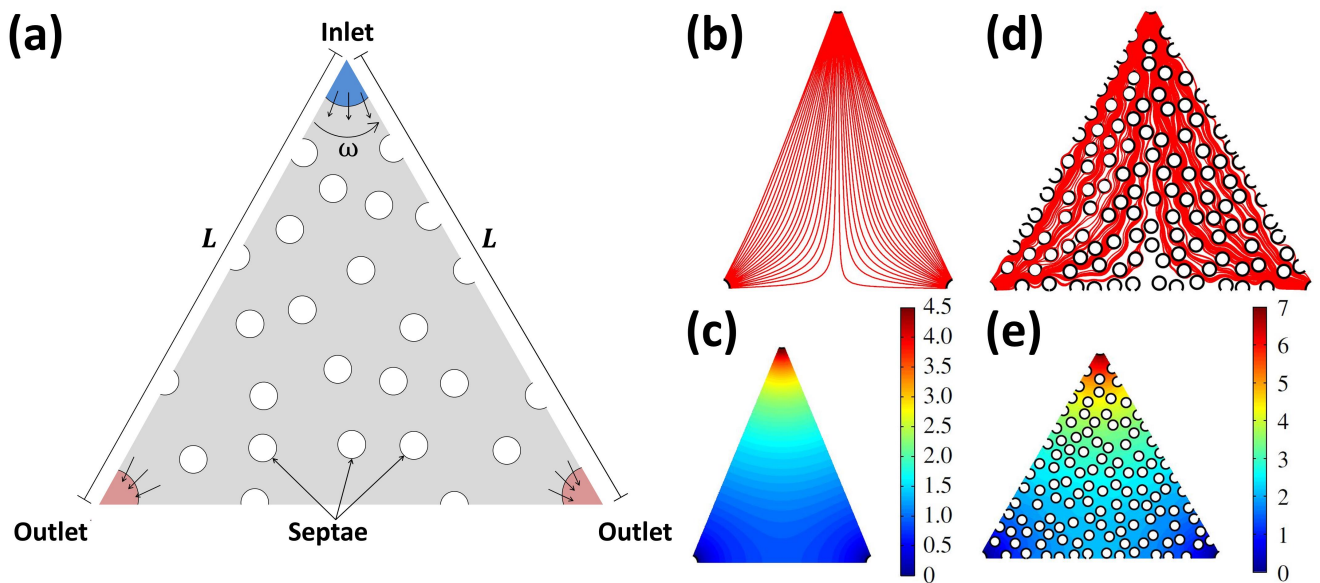


Figure 4: Zouache et al.'s model of blood flow in the choriocapillaris. (a) diagram to show the model geometry, including septae (represented by circles). Lobules are decomposed into isosceles triangular prisms, the inlet (top corner) being separated from the outlets (bottom corners) by sides of equal length (L). The internal angle at the inlet is denoted by ω . Figure adapted from Zouache et al. [131]. (b) and (c) flow streamlines (showing the paths followed by fluid particles, (b)) and pressure field (c) in the absence of septae ($\omega = 45^\circ$). (d) and (e) flow streamlines (d) and pressure field (e) in the presence of septae ($\omega = 60^\circ$). Figures (b)–(e) reproduced, with permission pending, from Zouache et al. [131].

be *passive*, driven by the pressure gradient between the inlet and outlets. Blood cells are not modelled explicitly, rather they are assumed to be passive tracers.

The model is used to determine how the *pressure drop* (between the inlet and outlets) and average fluid particle *residence time* (average time spent by blood corpuscles in the lobule) depend upon the internal angle at the inlet and the septae volume fraction.

In the absence of septae, a separation (stagnation) streamline divides the triangle in two, running from the inlet, to a stagnation point on the opposite side of the triangle, midway between the two outlets (see Figures 4(b) and (c)). The pressure drop is minimised, and the average residence time maximised, when the inlet angle is 90° , whilst the pressure drop increases and the residence time decreases as the inlet angle approaches 0 or 180° . The residence time is lower along streamlines close to the walls of the domain, and increases along streamlines approaching the stagnation streamline. As the septae volume fraction increases, the pressure drop and bulk flow velocity increase and the average residence time decreases (see Figures 4(d) and (e)). However, the septae also increase the residence time in the stagnation regions created on their surfaces where the streamlines separate.

As lobule geometry varies across the eye, so too does the pressure drop, blood velocity and residence time. It may be that this variation in geometry is the means by which the exchange of oxygen and other nutrients is modulated to match supply with demand. This *spatial variation* could also help to explain the geographical heterogeneity in vulnerability seen in retinal diseases such as *retinitis pigmentosa* (RP) and *age-*

related macular degeneration (AMD) [131]. It has been noted that drusen tend to form near venular openings in AMD [44]. This model suggests a possible explanation, since it predicts that the residence time of fluid particles is greatest here [131].

Whilst this model provides a useful first step in mathematically describing the CC, it has several limitations. In particular, it does not capture the movement of fluid between the CC and the retina, nor does it account for the three-dimensional nature of the flow, which could have a significant effect on residence time. Zouache et al. are now developing a 3D Navier-Stokes, advection-diffusion model to address these limitations [131]. A further interesting extension would be to couple models of the CC to models of the retina in disease states such as RP and AMD, where the supply of oxygen and other nutrients may be critical in driving the disease progression.

Zouache et al.'s work has also served to highlight shortcomings in existing experimental data. In particular, the interior angle at the inlet has not been investigated and, as yet, only one measurement for the pressure drop between inlet and outlet has been published. Zouache et al.'s models show that both of these features are of critical importance for blood flow within the CC and, as such, their accurate measurement should present a promising direction for future experimental research.

3.4. Photoreceptors

A number of models considering either individual photoreceptors or groups of photoreceptors in health have been developed. These models focus on processes such as retinal light adaptation, phototransduction [see in particular 65, 103, 115], photoreceptor and horizontal cell interactions, circadian rhythms

[19], information processing [105, 106] and receptive fields. Many of these studies are reviewed in Keener and Sneyd [60], Chapter 22, to which the reader is referred for further details.

Here we discuss more recent work by Macdougall [74] which provides a potential explanation for the observed *diurnal variation in rod photoreceptor outer segment (OS) length*. Each rod OS is composed of a stack of approximately 700–1200 membranous *discs* [122]. Discs are continuously replenished from the base of the OS, where it meets the IS, whilst groups of discs at the outer tip of the OS are intermittently shed and subsequently phagocytosed by the underlying RPE, the most significant shedding event occurring at the onset of LA [121, 122, 123, 124]. As a consequence, the OS is completely replaced over a period of 9–13 days [as measured in the rhesus monkey and assumed to hold true in humans 122]. Rod OS length varies over a daily cycle, growing under DA and shrinking under LA, indicating that the shedding and renewal rates vary with illumination [1].

Macdougall [74] construct three spatially-resolved continuum models, each testing a different hypothesis, proposed to explain the observed differences in OS length under DA and LA. The first model tests the hypothesis that the observed dynamics can be explained by changes in the *oxygen landscape* between DA and LA, whilst the second tests the hypothesis that the dynamics can be explained by changes in the *phosphocreatine shuttle-derived ATP* concentration in the OS between DA and LA. Both models fail in important respects (see below). Therefore, the third model proposes that a *combination* of changes in the oxygen and phosphocreatine shuttle-derived ATP concentrations is sufficient to explain the OS dynamics. All three models consist of PDEs and ODEs, where the PDEs are defined on a 1D domain spanning the region between the inner end of the IS and the outer end of the OS, the former boundary being fixed in space and the latter free to move (see Figure 5(a)). In each case, it is assumed that the choroid is the sole supplier of oxygen.

The first model consists of a PDE for oxygen concentration and an ODE for OS length. Oxygen diffuses freely across the photoreceptor and is taken up at a baseline level across the domain, with an additional consumption term in the IS to model mitochondrial uptake there, which increases under DA (see Section 3.1). The OS length increases or decreases at a rate proportional to the difference between a predefined *threshold concentration* and the oxygen concentration at the inner end of the IS. The length increases when the oxygen concentration at the inner tip of the IS is above the threshold (i.e. in abundance), and decreases when the oxygen concentration is below the threshold (i.e. in short supply).

The model admits unique, positive, steady-state solutions for OS length under both DA and LA. Simulations capture a 24-hour cycle, starting with the light adapted steady-state solution at $t = 0$ hours, followed immediately by DA, switching to LA at $t = 12$ hours. The only parameter which changes between DA and LA is the rate of oxygen uptake in the IS. It is found that OS length increases under LA and decreases under DA, behaviour which is the *reverse* of that seen *in vivo*. This result is robust under parameter sensitivity analysis and suggests that oxygen

cannot be the sole regulator of OS length.

The second model focusses on how the spatial distributions of creatine phosphate, creatine, free phosphate, ATP and ADP change over time and regulate OS length (see Figure 5(a)). ADP combines reversibly with phosphate to form ATP. The dominant source of ATP is assumed to be that formed by oxidative phosphorylation in the IS mitochondria, rather than that formed by glycolysis throughout the photoreceptor. Consequently, ATP production is neglected in the OS. Dephosphorylation is assumed to be negligible in the OS under DA. However, the demand for ATP in the OS increases under LA, such that dephosphorylation occurs under LA. The diffusion rates of ATP and ADP are slow and, hence, neglected. Therefore, in order for IS-produced ATP to reach the OS, it must do so via the *phosphocreatine shuttle*: creatine binds ATP reversibly to form creatine phosphate and ADP, the forward reaction being favoured in the IS and the reverse in the OS. Creatine phosphate, creatine and phosphate are all free to diffuse across the photoreceptor, resulting in a net flux of creatine phosphate from the IS to the OS, and of creatine and phosphate from the OS to the IS. Since the ATP and ADP concentrations evolve on a much faster timescale than those of the other reactants, they are assumed to be at quasi-steady-state, so the system comprises 3 PDEs for phosphocreatine, creatine and phosphate. The OS is assumed to grow at a constant rate and to shed discs only when the ATP concentration at the outer tip of the OS falls beneath a threshold value, corresponding to a *critical OS length*, at which point shedding proceeds at a rate proportional to the amount by which OS length exceeds this critical length.

Simulations for the 24 hour dark/light cycle predict that the OS will shed discs under LA, causing it to shrink towards a steady-state (after about 2 hours), in agreement with *in vivo* observations. The OS length increases linearly under DA; however, it does not reach steady-state, growing *unboundedly* if DA is maintained indefinitely. These results suggest that the phosphocreatine shuttle is sufficient to regulate OS length under LA, but not under DA.

The third model combines the hypotheses of the two previous models. Simulations of the combined model show OS growth under DA and shrinkage under LA, in agreement with *in vivo* observations (see Figure 5(b)). The decrease in IS oxygen consumption leads to growth under LA; however, rapid shedding dominates growth at the onset of LA [as observed in 123] leading to net OS shrinkage (see Figure 5(c)). The shedding rate subsequently decreases, balancing growth, such that the system approaches, and effectively reaches, steady-state under LA. Growth under DA is both linear and *bounded*, improving on both of the previous models; however, OS growth does not reach steady-state until approximately 100 hours. Whilst one would expect growth to stall earlier than this *in vivo*, these results are supported by a study carried out by Bassi and Powers [9] on goldfish, which showed that OS length increases at a constant rate when dark conditions are sustained for 7 days. In an ordinary light/dark cycle, the onset of LA interrupts growth under DA, such that continued growth beyond the physiological norm is not realised.

Many retinal diseases (e.g. AMD and RP) are associated

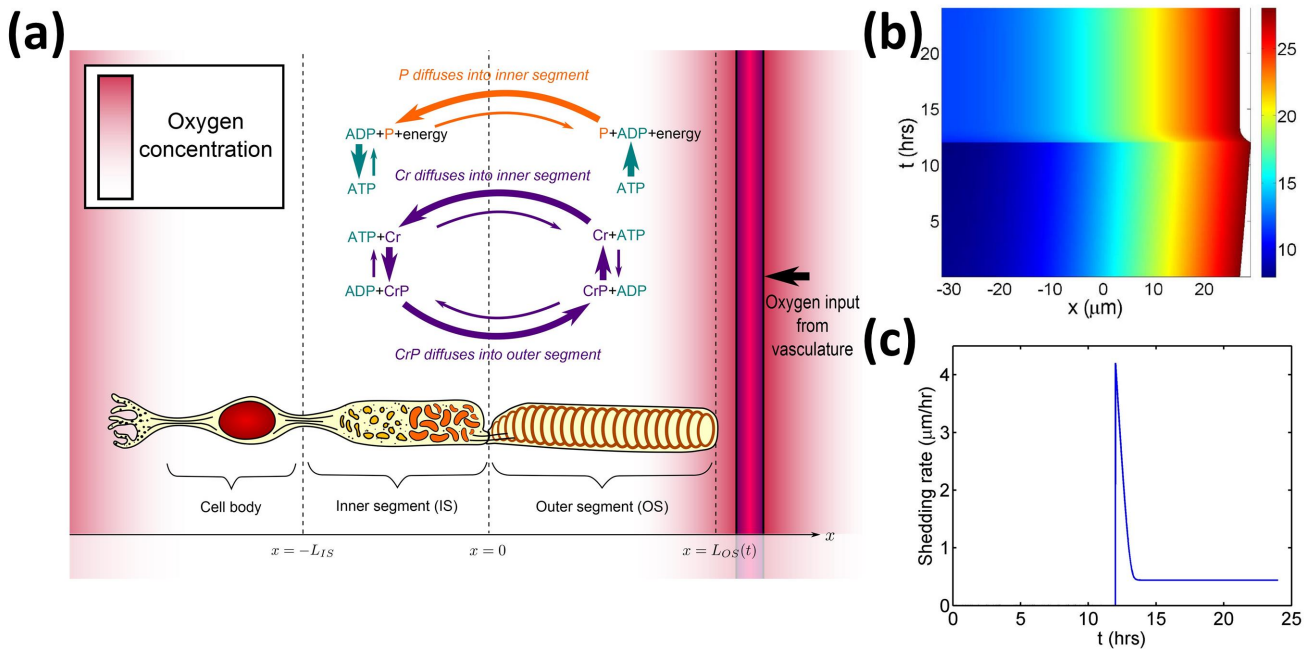


Figure 5: Macdougall’s model of photoreceptor shedding and regrowth. (a) diagram showing the model geometry, the oxygen distribution, and the kinetics and dynamics of the phosphocreatine shuttle. The photoreceptor IS has a fixed length, spanning the region between $x = -L_{IS} < 0$ and $x = 0$, whilst the OS length varies with time, t , spanning the region between $x = 0$ and $x = L_{OS}(t) > 0$. Oxygen, phosphocreatine (CrP), creatine (Cr) and phosphate (P) diffuse freely across the domain, whilst none of the species can leave the photoreceptor. Diffusive transport of ATP and ADP is neglected. ADP and P combine reversibly to form ATP, whilst CrP and ADP react reversibly to form Cr and ATP. Larger arrows show the dominant direction of each reaction. (b) simulation results for the third (combined) model, showing the growth and shrinkage of the OS over a 24 hour dark/light cycle, where the heat map represents the oxygen profile (in units of μM) internal to the photoreceptor. The simulation is initiated at the LA steady-state, grows under dark conditions for the first 12 hours and shrinks under light conditions from 12 to 24 hours. (c) graph to show the evolution of the shedding rate over time for the simulation depicted in (b). Shedding is absent under DA, but occurs under LA, reaching its highest rate shortly after the onset of LA. Figures (a) and (b) reproduced, with permission and modifications, from Macdougall [74], where the diagram of the photoreceptor in (a) is adapted from Young [121]. Figure (c) supplied by Macdougall and reproduced with permission.

728 with a decrease in OS length. One possible cause of decreased⁷⁵¹
 729 OS length is *mitochondrial inefficiency*, or inefficiency in OS
 730 *energy utilisation*. This may be represented in the model by⁷⁵²
 731 decreasing the IS ATP production rate or increasing the ATP⁷⁵³
 732 threshold. Both changes decrease OS length, suggesting that⁷⁵⁴
 733 these factors are sufficient to explain the OS shrinkage observed⁷⁵⁵
 734 in diseased states. The above inefficiencies could also be rep⁷⁵⁶
 735 resented by increasing the rate at which the ISs take up oxy⁷⁵⁷
 736 gen or reducing the oxygen threshold; however, this has an in⁷⁵⁸
 737 significant effect on OS length, since, although it decreases the⁷⁵⁹
 738 steady-state OS length, the steady-state is not reached during a⁷⁶⁰
 739 standard diurnal cycle. ⁷⁶¹

740 The above study illustrates the way in which mathematical⁷⁶²
 741 models can be used to isolate mechanisms in a way that would⁷⁶³
 742 be difficult, if not impossible, experimentally; examining their⁷⁶⁴
 743 sufficiency in explaining observed behaviours. Future models⁷⁶⁵
 744 could incorporate the effects of Ngf in oxygen transport (see⁷⁶⁶
 745 Section 3.2), or signalling between the photoreceptor and the⁷⁶⁷
 746 RPE [74]. The model could also be developed to consider dis⁷⁶⁸
 747 ease states. For example, it could be combined with the oxygen⁷⁶⁹
 748 toxicity mode for RP, described in Section 5.1.3, to account for⁷⁷⁰
 749 the increased oxidative damage incurred by the IS as they ap⁷⁷¹
 750 proach the choroid, following shrinkage of the OS. ⁷⁷²

4. Development

4.1. Retinal Angiogenesis

The retinal capillary layers, also known as the *retinal vas-*
cular plexus (RVP), colonize the retina via the process of *an-*
giogenesis (the development of new blood vessels from pre-
 existing vessels). *Astrocytes* migrate from the optic nerve, over
 the surface of the inner retina, in response to a gradient in *platelet-*
derived growth factor A (PDGF-A), which is produced by the
 underlying retinal ganglion cells. Astrocytes in turn guide the
 formation of the RVP, producing *vascular endothelial growth*
factor A (VEGF-A), which attracts *endothelial cells* to move up
 spatial gradients in its concentration, from the optic nerve, to-
 ward the retinal periphery. Astrocyte migration begins shortly
 before birth, whilst endothelial migration begins on *post-natal*
day 0 (P0), reaching the retinal periphery by P8 [6, 77, 119].

Aubert et al. [6], McDougall et al. [77] and Watson et al.
 [119] have created a series of models, produced alongside an
 accompanying experimental program, to capture the dynamics
 of the angiogenesis of the superficial RVP, in the developing
 murine (mouse) retina. The mammalian retina is an ideal sys-
 tem for studying angiogenesis, since the vascular architecture
 can easily be imaged using *retinal whole mounts*. Furthermore,
 development can be split into a well-defined sequence of events

774 and the vessel network has an ordered architecture, facilitating⁸³¹
775 comparisons between *in vivo* and *in silico* results.⁸³²

776 In Aubert et al. [6], two 1D PDE models are developed, de-⁸³³
777 fined on a domain spanning the region between the centre of⁸³⁴
778 the optic nerve and the position of the retinal periphery once⁸³⁵
779 fully-grown, starting from P0 (for model 1) or E17 (*embryo*-⁸³⁶
780 *onic day 17*, or P-4, for model 2) and running to P8. The first⁸³⁷
781 model focusses on capillary tip density, blood capillary density⁸³⁸
782 (which follow behind the capillary tips) and VEGF-A concen-⁸³⁹
783 tration, whilst the second accounts also for astrocyte density⁸⁴⁰
784 and PDGF-A concentration.⁸⁴¹

785 In the first model, an initial VEGF-A gradient is imposed,⁸⁴²
786 whilst in the second, the VEGF-A gradient is initially set to⁸⁴³
787 zero, and evolves over time as it is produced by astrocytes and⁸⁴⁴
788 consumed by endothelial cells, matching the *in vivo* situation⁸⁴⁵
789 more closely. Sensitivity analysis of the first model shows that⁸⁴⁶
790 *chemotaxis* has a significant influence upon RVP development,⁸⁴⁷
791 confirming the importance of the more realistic chemotactic⁸⁴⁸
792 gradients in the second model. The simulation predictions for⁸⁴⁹
793 capillary tip and astrocyte migration from the second model are⁸⁵⁰
794 in good agreement with the *in vivo* results, providing experi-⁸⁵¹
795 mental support for the model and showing that the factors ac-⁸⁵²
796 counted for in the model are sufficient to explain the observed⁸⁵³
797 dynamics.⁸⁵⁴

798 In later work, a 2D *hybrid model* was used to simulate the⁸⁵⁵
799 complex, branched structure of the RVP [77, 119]. The model⁸⁵⁶
800 contains discrete-stochastic and continuous-deterministic ele-⁸⁵⁷
801 ments and is posed on a domain spanning the surface of the⁸⁵⁸
802 inner retina. As before, PDEs are defined for the astrocyte and⁸⁵⁹
803 endothelial cell densities (the distinction between capillary tips⁸⁶⁰
804 and blood capillaries being dropped at the level of the PDEs)⁸⁶¹
805 and for the PDGF-A and VEGF-A concentrations. Four ad-⁸⁶²
806 ditional PDEs are also included to account for the density of⁸⁶³
807 the matrix-bound proteins *vitronectin* and *fibronectin*, both of⁸⁶⁴
808 which are produced by astrocytes, and the concentrations of⁸⁶⁵
809 astrocyte and endothelial cell produced *matrix degrading en-*⁸⁶⁶
810 *zymes*, which degrade vitronectin and fibronectin respectively.⁸⁶⁷
811 Astrocytes and endothelial cells move up adhesion gradients in⁸⁶⁸
812 vitronectin and fibronectin respectively, via *haptotaxis* (see Fig-⁸⁶⁹
813 ure 6(a)).⁸⁷⁰

814 In order to capture the migration of individual astrocytes⁸⁷¹
815 and endothelial cells, and hence the formation of discrete cap-⁸⁷²
816 illary vessels, the PDEs for these equations are discretised. The⁸⁷³
817 direction of movement of each individual cell is determined⁸⁷⁴
818 stochastically, integrating the effects of *diffusion* (random move-⁸⁷⁵
819 ment), *chemotaxis* and *haptotaxis*. Both astrocytes and endothe-⁸⁷⁶
820 lial cells also undergo stochastic branching, the probability of⁸⁷⁷
821 *branching* increasing with increasing PDGF-A and VEGF-A⁸⁷⁸
822 concentrations respectively, whilst *anastomoses* occur when-⁸⁷⁹
823 ever a sprout tip meets either another sprout tip or an existing⁸⁸⁰
824 capillary.⁸⁸¹

825 Blood is a *biphasic* fluid, composed largely of erythrocytes⁸⁸²
826 and plasma. The model accounts for the separation of these two⁸⁸³
827 phases at bifurcations in the vascular bed. The model also ac-⁸⁸⁴
828 counts for changes in vessel radius due to wall shear stress, in-⁸⁸⁵
829 travascular pressure, conducted and convected metabolic stim-⁸⁸⁶
830 uli and a shrinking tendency which dominates in the absence of⁸⁸⁷

growth stimuli. The *conducted* (acting upstream) and *convected*
(acting downstream) *stimuli* help to prevent *shunt formation* by
favouring the dilation of vessels that are part of extended flow
pathways.

Lastly, the model contains PDEs to describe the oxygen dy-
namics in the tissues and within the blood vessels. It is also as-
sumed that erythrocytes are the only source of oxygen. *Vessel*
pruning occurs when the oxygen concentration in the surround-
ing tissue and vessel age exceed critical thresholds and in the
absence of any flow-related stimuli.

Simulations including astrocyte and endothelial cell migra-
tion, but neglecting perfusion, produce cell front migratory dy-
namics that match well with *in vivo* experiments (see Figure
6(c)); however, they do not reproduce the highly structured vas-
cular trees seen *in vivo*. When perfusion, plexus remodelling
and oxygen delivery, without convected and conducted stimuli,
are included, capillary shunts develop, such that the *haemat-*
ocrit only takes non-zero values in the regions neighbouring the
optic nerve. As a result, oxygen delivery to the peripheral retina
is negligible. When convected and conducted stimuli are in-
cluded (see Figure 6(d)), the haematocrit is spatially heteroge-
neous, and the entire retina receives a reasonable supply of oxy-
gen, demonstrating the importance of these stimuli for adequate
oxygen delivery. Interestingly, the haematocrit is predicted to
increase toward the retinal periphery, exceeding 0.75 in some
regions around the periphery (this is as compared with the in-
put value of 0.45), in good agreement with Ganesan et al. [45]
(see Section 3.1) and being most highly concentrated around
dilated arterio-venous loops. This phenomenon is due to *phase*
separation, which causes the haematocrit to increase along the
arterial side of each bifurcation. In the absence of phase separa-
tion, the peripheral retina would be oxygen starved. Also in
agreement with Ganesan et al. is the development of arterial in-
let segments that are narrower than those of the venous outlet
segments. Visual comparison of *in vivo* and *in silico* *vascular*
architectures reveals that they are qualitatively similar, the main
differences being that *in silico*, the vascular plexuses are a little
denser and the vessels remain dilated up to the growth front,
rather than narrowing toward the periphery (see Figure 6(b)).

Having benchmarked their model against normal develop-
ment, it can be used to predict what would happen if one or
more developmental mechanisms were altered. For example,
increasing or decreasing the VEGF-A diffusion coefficient 10-
fold slows the rate of capillary growth, due to the loss of sharp
gradients in VEGF, suggesting that the usual *isoform* (VEGF-
A₁₆₄) is more effective for retinal angiogenesis than its lighter
and faster diffusing (VEGF-A₁₂₀), and its heavier and slower
diffusing (VEGF-A₁₈₈) isoforms.

Increasing the input arterial haematocrit, or decreasing the
tissue oxygen consumption rate causes large capillary-free zones
and hyperoxia to develop, these effects being more extensive in
the latter case. The former case is equivalent to *retinopathy of*
prematurity and the latter to *oxygen-induced retinopathy*.

If capillary pruning is reduced, the spatial distribution of di-
lated vessels is not significantly affected, but phase separation
is reduced, causing haematocrit levels across the retina to be-
come more heterogeneous, with erythrocytes being more con-

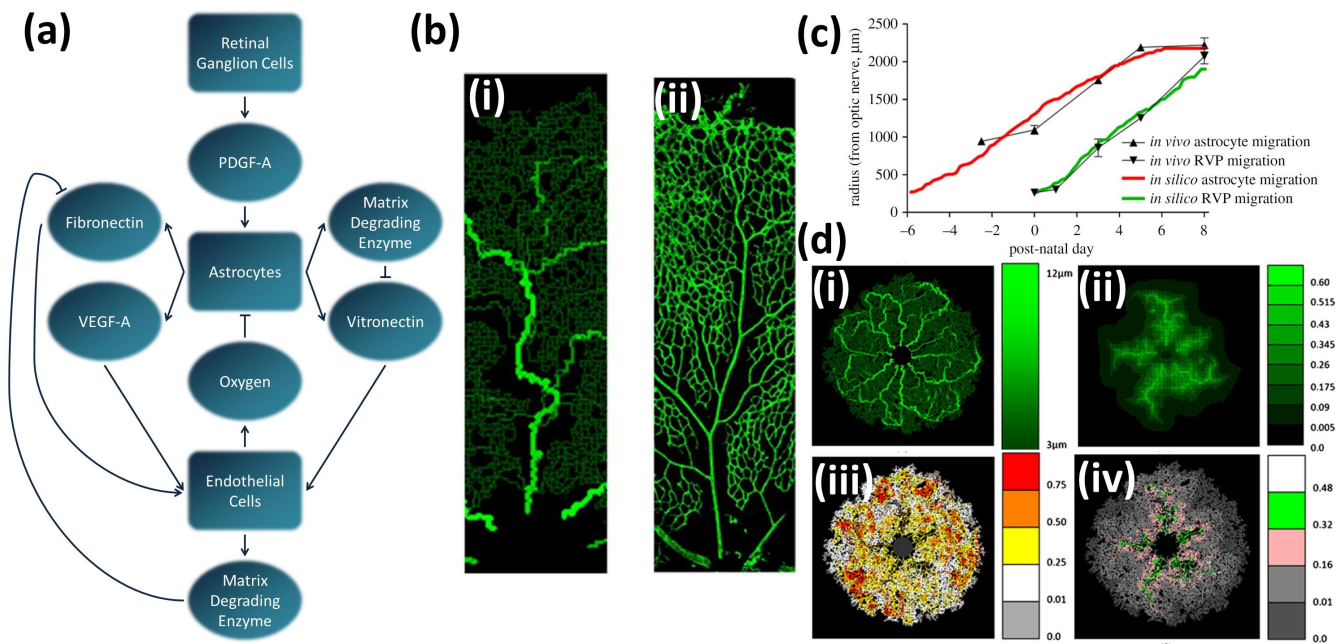


Figure 6: McDougall and co-workers' hybrid model of retinal angiogenesis [77, 119]. (a) diagram summarising the key components and processes included in the model. Pointed arrows indicate production or attraction, whilst flat-headed arrows represent degradation or inhibition. Figure adapted from McDougall et al. [77]. (b) comparison between *in silico* (i) and *in vivo* (ii) vasculatures at P7.7 and P8 respectively (using the full model). Brighter colour in the *in silico* image represents wider vessels, corresponding with the colour bar in (d)(i). The results are qualitatively similar, the main differences being that, *in silico*, the vascular plexuses are slightly denser and the vessels remain dilated up to the growth front, rather than narrowing toward the periphery. Figure reproduced, with permission pending, from Watson et al. [119]. (c) graph comparing the *in vivo* and *in silico* (neglecting perfusion) migration of astrocyte and endothelial cell fronts. The *in vivo* results are represented by black triangles (upward: astrocytes, inverted: endothelial cells), whilst the *in silico* results are represented by red (astrocytes) and green (endothelial cells) lines. The results show good agreement. Figure reproduced, with permission pending and modifications, from Watson et al. [119]. (d) simulation results from the full model at P7.7 showing (i) vessel radii, (ii) tissue oxygen concentration, (iii) haematocrit and (iv) vessel oxygen concentration. Figure reproduced, with permission, from McDougall et al. [77]. PDGF-A: platelet-derived growth factor A, VEGF-A: vascular endothelial growth factor A, P: post-natal day, RVP: retinal vascular plexus.

centrated around the dilated arteriolar segments. These results suggest that capillary pruning is important in ensuring that all regions of the retina receive an adequate supply of oxygen.

The above results illustrate how computational models can be used to examine scenarios and isolate mechanisms in a way that would be technically challenging, if not impossible, to reproduce experimentally. This is particularly true for the simulations in which the convected and conducted stimuli are switched off.

Extending the hybrid mode to 3D would allow studies of later developmental stages (between P8 and P16), during which vertical sprouting from the superficial RVP leads to the formation of two additional RVP layers deeper within the retinal tissue [77, 119]. This would require a fully 3D model. It would also be interesting to test whether the model could be adapted to account for the curved vascular arcades seen in humans (as opposed to the radial pattern found in the murine retina). The effects of mechanical signalling upon vessel formation and maturation could also be incorporated. Lastly, the model could be adapted to study *diabetic retinopathy* and the *critical developmental period* in the early stages of RP [79], providing a tool for testing potential treatment strategies.

Finally, we note that recent modelling studies have also considered angiogenesis within the cornea [see, 31, 54].

4.2. Retinal Mosaic Formation and Retinogenesis

A number of theoretical modelling studies have explored the formation of retinal photoreceptor and ganglion cell *mosaics*, using a combination of phenomenological and mechanistic approaches. Typically focussing on the processes of lateral migration, cell fate and cell death, these studies seek to explain how a regular arrangement of neurons emerges from an initially random distribution. These studies are reviewed in detail in Eglén [36, 37], to which the reader is referred for further details.

More recently, Salbreux et al. [97] have developed a computational model to explain the ordered packing of cone photoreceptors in the zebrafish retina, in terms of the coupling of mechanical deformations and planar cell polarity. Their model reproduces many behaviours observed during development *in vivo*, as well as elucidating how this process may break down in mutants. In addition, Jiao et al. [58] have constructed a multi-scale model for the packing of avian photoreceptors. The model indicates that short- and long-range repulsive forces between photoreceptors are sufficient to explain the observed patterns.

Barton and Fendrik [8] have used a stochastic model to explore vertebrate *retinogenesis*, the process by which different retinal cell types derive from multipotent retinal progenitor cells. The model, which assumes that a single factor regulates

936 both division and competency, reproduces the timings at which⁹⁸⁷
937 different cell types are produced, as measured in rats, suggest⁹⁸⁸
938 ing that a single regulatory factor is sufficient to explain this⁹⁸⁹
939 process.

940 5. Disease

941 The various diseased and damaged states of the retina have⁹⁹⁴
942 received a significant proportion of the theoretical modelling⁹⁹⁵
943 community's attention. Models cover a range of topics includ⁹⁹⁶
944 ing laser-induced damage [114], blast injury [95], retinal de⁹⁹⁷
945 tachment [57, 80], proliferative retinopathy [75, 76], retinitis⁹⁹⁸
946 pigmentosa and age-related macular degeneration. In what fol⁹⁹⁹
947 lows, we focus on the latter two conditions, where modelling¹⁰⁰⁰
948 studies are most highly concentrated.

949 5.1. Retinitis Pigmentosa

950 The term *retinitis pigmentosa* (RP) denotes a group of in¹⁰⁰⁴
951 herited retinal diseases which cause the progressive degener¹⁰⁰⁵
952 ation of photoreceptors and, hence, loss of vision. The most¹⁰⁰⁶
953 common inherited retinal degeneration, RP is currently untreat¹⁰⁰⁷
954 able [100]. RP usually occurs as a *rod-cone dystrophy*, in which¹⁰⁰⁸
955 rod function and number are diminished earlier and more severely¹⁰⁰⁹
956 than for cones [49]. *Cone-rod dystrophies*, in which cone loss¹⁰¹⁰
957 precedes rod degeneration, can also occur and, rarely, rod and¹⁰¹¹
958 cone loss may occur *simultaneously* [51]. Whilst the initial loss¹⁰¹²
959 of rods (or cones) may be attributed to genetic mutations, the¹⁰¹³
960 cause of the secondary loss of cones (or rods) is unknown.

961 Histological studies in humans and rats suggest that pho¹⁰¹⁵
962 toreceptor degeneration initiates in *patches*, which presumably¹⁰¹⁶
963 spread and coalesce over time [24, 47, 56, 66, 130]. RP pro¹⁰¹⁷
964 gression in animal models is largely homogeneous in space;¹⁰¹⁸
965 however, in humans, photoreceptor loss has a distinct *spatio*¹⁰¹⁹
966 *temporal pattern*, typically initiating in the mid-periphery, with¹⁰²⁰
967 the central retina being the last region to degenerate [51]. While¹⁰²¹
968 the phenomena driving this pattern remain to be determined,¹⁰²²
969 three hypotheses have been proposed to explain them: the *trophic*¹⁰²³
970 *factor*, *toxic substance* and *oxygen toxicity hypotheses*. Mathe¹⁰²⁴
971 matical modelling has proven valuable in evaluating the strengths¹⁰²⁵
972 and weaknesses of these hypotheses and in suggesting potential¹⁰²⁶
973 treatment strategies.

974 5.1.1. The Trophic Factor Hypothesis

975 It has been suggested that rods may release chemicals that¹⁰³⁰
976 are essential for cone survival [41, 82, 83, 84]. Rod loss would¹⁰³¹
977 remove the source of these factors, leading to cone degener¹⁰³²
978 ation. One such factor, *rod-derived cone viability factor* (Rd¹⁰³³
979 CVF), identified by Léveillard et al. [67], has been shown to¹⁰³⁴
980 slow cone degeneration and to preserve cone function in chick,¹⁰³⁵
981 mouse and rat models [41, 67, 82, 83, 84, 120].

982 Camacho, Wirkus *et al.* have developed a series of *spatially*¹⁰³⁷
983 *averaged* ODE models to investigate the role of RdCVF in both¹⁰³⁸
984 the healthy and diseased retinas.

985 Their first model considers the healthy retina, describing the¹⁰⁴⁰
986 dynamics of rod and cone OS number, and RPE cell number¹⁰⁴¹

[equivalent to the trophic pool, 20, note that we use the interpre⁹⁹⁰
991 tation given in the subsequent papers]. Their equations describe⁹⁹²
992 the shedding and renewal of the photoreceptor OS, where the⁹⁹³
993 renewal involves the conversion of trophic pool (which is con⁹⁹⁴
994 tinuously replenished) into new OS discs. Rods produce Rd⁹⁹⁵
995 CVF, which is mathematically distinct from the trophic pool, at⁹⁹⁶
996 no cost to themselves, augmenting the supply of trophic factor⁹⁹⁷
997 to the cones (see Figure 7(a)). The presence of RdCVF makes⁹⁹⁸
998 it possible for rods and cones to coexist indefinitely, suggest⁹⁹⁹
999 ing that this factor may be necessary for their mutual survival¹⁰⁰⁰
1000 [20]. We note that earlier modelling work by Camacho and col¹⁰⁰¹
1001 leagues led them to predict the existence of such a factor, before¹⁰⁰²
1002 its discovery by Léveillard et al. in 2004 [see 30], though they¹⁰⁰³
1003 were not the first to predict such a factor [82, 84].

1004 Mathematical analysis and numerical simulations suggest¹⁰⁰⁴
1005 that, for certain parameter values, the system will exhibit mul¹⁰⁰⁵
1006 tiple *stable oscillatory solutions*, of various amplitudes, corre¹⁰⁰⁶
1007 sponding to the rhythmic shedding and renewal of photorecep¹⁰⁰⁷
1008 tors observed *in vivo* (see Figure 7(b)). The period of oscillation¹⁰⁰⁸
1009 ranges from 8–9 hours, for small amplitude oscillations, to 26¹⁰⁰⁹
1009 hours, for large amplitude oscillations. The range of parame¹⁰¹⁰
1010 ters for which this behaviour occurs is larger, and hence these¹⁰¹⁰
1011 dynamics are more probable, when more RdCVF is produced¹⁰¹¹
1011 by rods and when photoreceptors convert trophic factor into OS¹⁰¹²
1012 more efficiently. Outside this parameter range, rods, cones and¹⁰¹²
1013 RPE cannot coexist.

1014 The model further predicts that rod and cone OS lengths os¹⁰¹⁵
1015 cillate *in phase*. This has been observed *in vivo*, but is not true¹⁰¹⁵
1016 of all species [see 20, and references therein]. It would be inter¹⁰¹⁶
1017 esting to investigate ways in which the model might be modified¹⁰¹⁷
1018 to induce *out-of-phase* oscillations, for example, by introducing¹⁰¹⁸
1019 an *explicit time delay* in the aid supplied to the cones via Rd¹⁰¹⁹
1019 CVF, capturing the *in vivo* delay [20].

1020 Camacho and Wirkus [22] extended their model to describe¹⁰²⁰
1021 the disease state of RP by distinguishing between *normal* and¹⁰²¹
1022 *mutant rods*, where both types of rod are genotypically mutant,¹⁰²²
1023 but only the latter type has had its functionality compromised¹⁰²³
1024 (represented in the model by altered rates of shedding and re¹⁰²⁴
1025 newal of OS). Normal rods can become mutant, but not vice¹⁰²⁵
1025 versa, whilst both normal and mutant rods consume trophic fac¹⁰²⁶
1026 tor and contribute RdCVF to the cones. The RPE equation is¹⁰²⁶
1027 also modified so that, neglecting the terms involving photore¹⁰²⁷
1028 ceptors, it obeys logistic, rather than exponential, dynamics, the¹⁰²⁸
1029 number of RPE cells remaining bounded under all conditions¹⁰²⁹
1029 (see Figure 7(a)).

1030 Mathematical analysis reveals that, for any given set of pa¹⁰³⁰
1031 rameter values, there exist seven *equilibrium* (steady-state) *so*¹⁰³¹
1032 *lutions*, each corresponding to a different stage in the disease¹⁰³²
1033 progression, from healthy to completely degenerate. Four pa¹⁰³³
1034 rameters, which are key in determining the form of the disease¹⁰³⁴
1035 progression, are identified, namely the *ratio of shedding to re*¹⁰³⁵
1036 *newal* in normal rods, mutant rods and cones, and the *carrying*¹⁰³⁶
1037 *capacity* of the RPE (in the absence of photoreceptors). All¹⁰³⁷
1038 of these parameters must remain fixed in order for an equi¹⁰³⁸
1039 librium solution to remain stable, whilst changes in parameter¹⁰³⁹
1040 values can drive disease progression between the different equi¹⁰⁴⁰
1041 librium solutions, where equilibrium solutions exchange stabil¹⁰⁴¹
1042 ity.

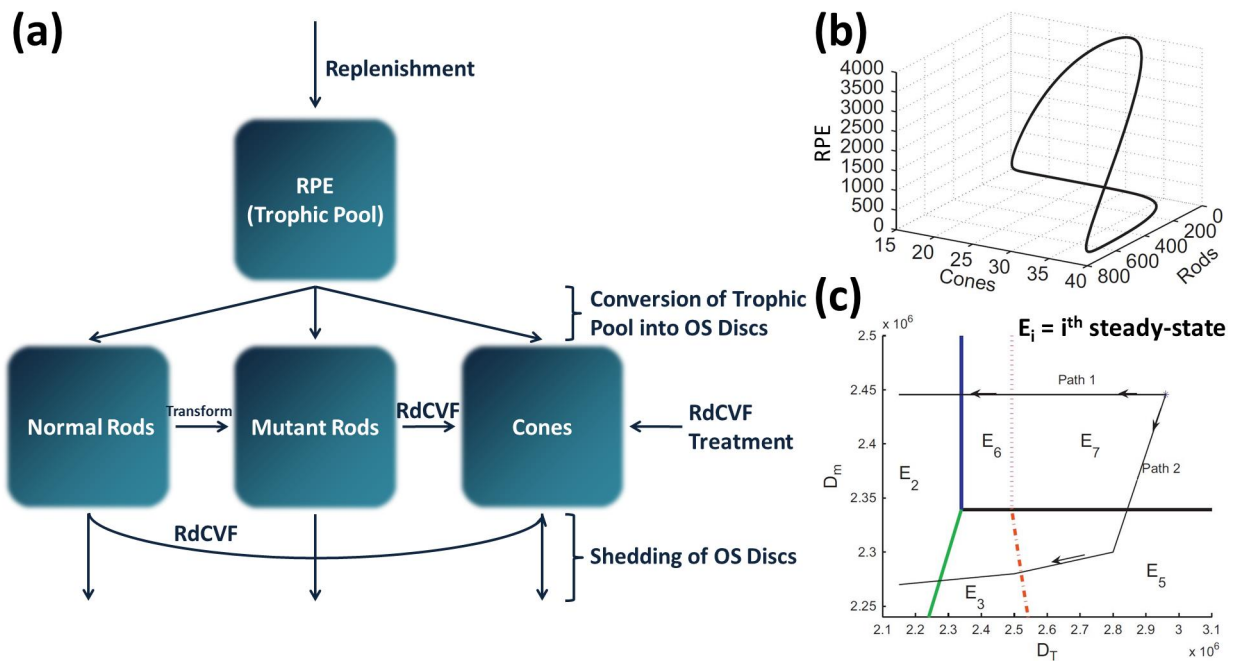


Figure 7: Camacho and Wirkus *et al.*'s trophic factor model of RP. (a) diagram showing the components and processes in the Camacho et al. [21] model. (The Camacho and Wirkus [22] model does not include RdCVF treatment, whilst the Camacho et al. [20] model includes neither treatment, nor the mutant rod component and its associated processes.) Figure adapted from Camacho et al. [20] and Camacho and Wirkus [22]. (b) *stable limit cycle* (oscillatory) solution of the Camacho et al. [20] model, demonstrating the rhythmic shedding and regrowth of rod and cone OS in the healthy retina. Figure reproduced, with permission and modifications, from Camacho et al. [20]. (c) diagram showing two alternative paths (marked with arrows) that may be traced through parameter space, leading to different cone-rod dystrophy forms of the RP disease progression, in the Camacho and Wirkus [22] model. Lines without arrows demarcate the boundaries of the stability regions, across which (transcritical) bifurcations occur. Path 1: $E_7 \rightarrow E_6 \rightarrow E_2$. Path 2: $E_7 \rightarrow E_5 \rightarrow E_3 \rightarrow E_2$. D_m : shedding to renewal ratio of mutant rods, D_T : RPE (trophic pool) carrying capacity, E_7 : healthy steady-state, E_6 : steady-state at which all cones are lost, E_5 : steady-state at which all normal rods are lost, E_3 : steady-state at which all cones and normal rods are lost, E_2 : steady-state at which all photoreceptors are lost. Figure reproduced, with permission and modifications, from Camacho and Wirkus [22].

ity through (transcritical) *bifurcations*. Variation of these pa₁₀₄₄
 rameters allows a variety of paths to be traced to total blind₁₀₄₅
 ness, passing through different combinations of equilibrium so₁₀₄₆
 lutions, corresponding either to the rod-cone, cone-rod or si₁₀₄₇
 multaneuous form of RP (see Figure 7(c)).₁₀₄₈

The above results suggest potential *therapeutic strategies*₁₀₄₉
 that could halt disease progression. For example, the model₁₀₅₀
 predicts that progression of rod-cone RP requires a decrease in₁₀₅₁
 the ratio of shedding to renewal in cones. Therefore, a treatment₁₀₅₂
 designed to maintain this ratio might prevent disease progres₁₀₅₃
 sion in patients whose rods and cones are degenerating via thi₁₀₅₄
 s pathway.₁₀₅₅

This model generated two other, noteworthy results. Firstly₁₀₅₆
 small changes in parameter values can lead to markedly differ₁₀₅₇
 ent pathways to blindness, helping to explain the differences₁₀₅₈
 in disease progression seen in closely related patients with the
 same mutation. For example, an increase in the ratio of shed₁₀₅₉
 ding to renewal in cones can change the disease progression₁₀₆₀
 from one in which all photoreceptors are lost simultaneously₁₀₆₁
 to one in which cones are lost before rods. Secondly, the model₁₀₆₂
 suggests that the reduction in photoreceptor OS length observed₁₀₆₃
 in RP is an *emergent property* of the nonlinear interactions be₁₀₆₄
 tween rods, cones and RPE, rather than simply due to changes₁₀₆₅
 in shedding and renewal rates.₁₀₆₆

Lastly, Camacho et al. [21] modified their RP model to include an RdCVF treatment term (see Figure 7(a)). Using *optimal control theory*, they determined a treatment level that will achieve the desired degree of cone preservation, whilst minimising the RdCVF dose. This is important, since using too large a dose of RdCVF could impair retinal function. A two week treatment period is considered for comparison with Léveillard et al. [67]'s experimental results. Simulations, starting from different stages in the disease progression, reveal that treatment will have a negligible effect on rod loss, but can significantly reduce cone loss during the later stages of the disease (when all the rods have been lost), provided the treatment is aggressive enough. It is also possible, using the model, to estimate the minimum treatment required to achieve the approximate 40% sparing of cones reported in Léveillard et al. [67].

5.1.2. The Toxic Substance Hypothesis

Another mechanism by which photoreceptor cell death could spread is via the release of toxic substances by dying photoreceptors. These substances are most likely released into the interphotoreceptor matrix, where they are taken up by and, thus, poison neighbouring photoreceptors. It has been suggested that toxic substances may be transmitted between photoreceptors via gap junctions; however, this hypothesis is now in doubt,

1091 since disruption of gap junctions does not seem to affect dis¹¹⁴⁸
1092 ease progression [63, 91].¹¹⁴⁹

1093 Clarke et al. [25] have suggested a *one-hit model* of neu¹¹⁵⁰
1094 ronal cell death for a variety of conditions including RP [see¹¹⁵¹
1095 also 26, 27, 28]. Guided by experimental observations which¹¹⁵²
1096 suggest that the risk of (photoreceptor) cell death is either con¹¹⁵³
1097 stant or decreases exponentially with age, Clarke et al. [25] as¹¹⁵⁴
1098 sume that the time at which a neuron dies is random.¹¹⁵⁵

1099 This assumption can be justified at the biochemical level by¹¹⁵⁶
1100 the *mutant steady-state* (MSS) *hypothesis*, which suggests that¹¹⁵⁷
1101 mutations result in elevated levels of a pre-apoptotic compound¹¹⁵⁸
1102 placing it closer to a critical threshold, above which apoptosis¹¹⁵⁹
1103 is induced [28]. Random fluctuations in the concentration of¹¹⁶⁰
1104 this compound may cause it to exceed this threshold, resulti¹¹⁶¹
1105 ng in cell death [28].¹¹⁶²

1106 Burns et al. [18] incorporated the MSS hypothesis into a¹¹⁶³
1107 spatially explicit 1D model, consisting of a pair of PDEs, in¹¹⁶⁴
1108 which a diffusible *toxic factor*, produced by dying photorecep¹¹⁶⁵
1109 tors and released into the interphotoreceptor matrix, upregulates¹¹⁶⁶
1110 the production of *pre-apoptotic factors* in the surrounding pho¹¹⁶⁷
1111 toreceptors. Assuming that toxic factor uptake is effectively lin¹¹⁶⁸
1112 ear, the toxic factor PDE can be solved analytically, so that the¹¹⁶⁹
1113 problem reduces to solving a single PDE for the pre-apoptoti¹¹⁷⁰
1114 c factor. Since the pre-apoptotic factor is unable to move between¹¹⁷¹
1115 photoreceptors, its PDE lacks terms for diffusion or transport¹¹⁷²
1116 containing only kinetic terms. Thus, it may be split into N spa¹¹⁷³
1117 tially dependent ODEs, one for each of the N photoreceptors¹¹⁷⁴
1118 spanning the domain.¹¹⁷⁴

1119 In the absence of toxic factor, each of the ODEs is *bistable*,¹¹⁷⁵
1120 such that the pre-apoptotic factor concentration can exist sta¹¹⁷⁶
1121 bly at either of two steady-state values (see Figure 8(a)). The¹¹⁷⁷
1122 solution with the lower value (zero) corresponds to the MSS,¹¹⁷⁸
1123 in which all photoreceptors are assumed to start, whilst the¹¹⁷⁹
1124 upper (strictly positive) value corresponds to a state in which¹¹⁸⁰
1125 the photoreceptor is committed to apoptosis. These two sta¹¹⁸¹
1126 ble steady-states are separated by an unstable steady-state. In¹¹⁸²
1127 creases in the concentration of the toxic factor above a *critical*¹¹⁸³
1128 *threshold* cause the lower stable and unstable steady-states to¹¹⁸⁴
1129 approach one another, coalesce and annihilate, such that the up¹¹⁸⁵
1130 per stable steady-state becomes the attractor for the whole sys¹¹⁸⁶
1131 tem. Provided the toxic factor concentration remains elevated¹¹⁸⁷
1132 for long enough, the system will become irreversibly trapped in¹¹⁸⁸
1133 this steady-state's *basin of attraction* (such that it continues to¹¹⁸⁹
1134 move towards the steady-state), at which point the photorecep¹¹⁹⁰
1135 tor is considered to be *committed to apoptosis*.¹¹⁹¹

1136 A stochastic simulation algorithm is used to determine when¹¹⁹²
1137 a photoreceptor in the commitment state will undergo apopto¹¹⁹³
1138 sis, where the lifetime of each photoreceptor in the commitmen¹¹⁹⁴
1139 t state is drawn from either a normal or an exponential distribu¹¹⁹⁵
1140 tion. Upon apoptosis, a photoreceptor releases toxic factor into¹¹⁹⁶
1141 the extracellular space where it evolves over time according to¹¹⁹⁷
1142 the analytical solution to its associated PDE. The degeneration¹¹⁹⁸
1143 process is initiated by selecting a single photoreceptor to un¹¹⁹⁹
1144 dergo apoptosis. When the lifetime in the commitment state¹²⁰⁰
1145 is normally distributed, the decline in photoreceptor number¹²⁰¹
1146 is slow and sigmoidal. However, when it is *exponentially dis*¹²⁰²
1147 *tributed*, photoreceptors are lost more rapidly, declining expo-

1148 nentially, in agreement with the experimental studies mentioned
1149 above [25, 28]. This suggests that photoreceptor lifetimes in the
1150 apoptosis commitment state are exponentially, rather than nor-
1151 mally, distributed. Simulations also demonstrated that when
1152 multiple photoreceptors undergo apoptosis at points that are
1153 close in space and time, the released toxic factors may have
1154 a *synergistic* effect, committing more photoreceptors to apop-
1155 tosis than would occur if the effects were more separated (see
1156 Figure 8(b)).

The model also predicts a *patchy pattern* of photoreceptor
1157 loss, similar to that often observed in the early stages of RP
1158 (see above), with patch diameters similar to those seen *in vivo*,
1159 providing a potential explanation for these patterns (see Figure
1160 8(c)).

1161 More recently, Lomasko et al. [71, 72] and Lomasko and
1162 Lumsden [73] have extended the work of [18] by constructing
1163 stochastic models of cytoskeleton-induced neuron death. While
1164 these models were not developed specifically for the retina, it
1165 is noteworthy that they replicate the exponential and sigmoidal
1166 patterns of cell loss measured by Clarke et al. [25].

5.1.3. The Oxygen Toxicity Hypothesis

The final hypothesis suggests that the initial loss of pho-
1167 toreceptors results in a rise in oxygen levels, due to decreased
1168 demand, creating a toxic environment for those that remain
1169 [109, 116, 117]. These oxygen levels are maintained, since the
1170 CC, which is the main source of oxygen for the photorecep-
1171 tor containing outer retina, autoregulates poorly in response to
1172 hyperoxia [109, 125, 128]. An increase in oxygen levels above
1173 normal physiological levels (normoxia) is harmful to retinal tis-
1174 sue, since it upsets the redox potential, resulting in increased
1175 production of *reactive oxygen species* which cause damage to
1176 lipids, protein and DNA [2, 3, 62, 99].

1177 Roberts [92] has created a series of models examining the
1178 *oxygen toxicity hypothesis*. The models are formulated as sys-
1179 tems of PDEs, for oxygen concentration, photoreceptor density
1180 (or rod and cone densities taken separately) and capillary (CC)
1181 surface area per unit volume. The models incorporate the het-
1182 erogeneous distribution of rods and cones, whilst a spherical
1183 polar coordinate system is used to capture the geometry of the
1184 eye. For simplicity, the retina is assumed to be symmetric in
1185 the azimuthal direction (for rotations about the axis, passing
1186 at a right-angle to the wall of the eye, through the foveal cen-
1187 tre) and hence the optic disc is neglected. Oxygen supplied
1188 by the CC diffuses freely across the domain and is consumed
1189 by photoreceptors at a rate proportional to their density, whilst
1190 photoreceptors either remain at or approach their healthy local
1191 density under normoxia (unless they are absent, in which case
1192 their density remains at zero), but decay exponentially when
1193 local oxygen levels rise above a defined *hyperoxic threshold*.
1194 The CC dynamics follow those of the photoreceptors; however,
1195 since their rate of decay and regrowth is generally slower than
1196 that of the photoreceptors, their dynamics lag behind those of
1197 the photoreceptors.

The first set of models are posed on a 1D domain, spanning
1198 the region between the centre of the fovea and the ora serrata.

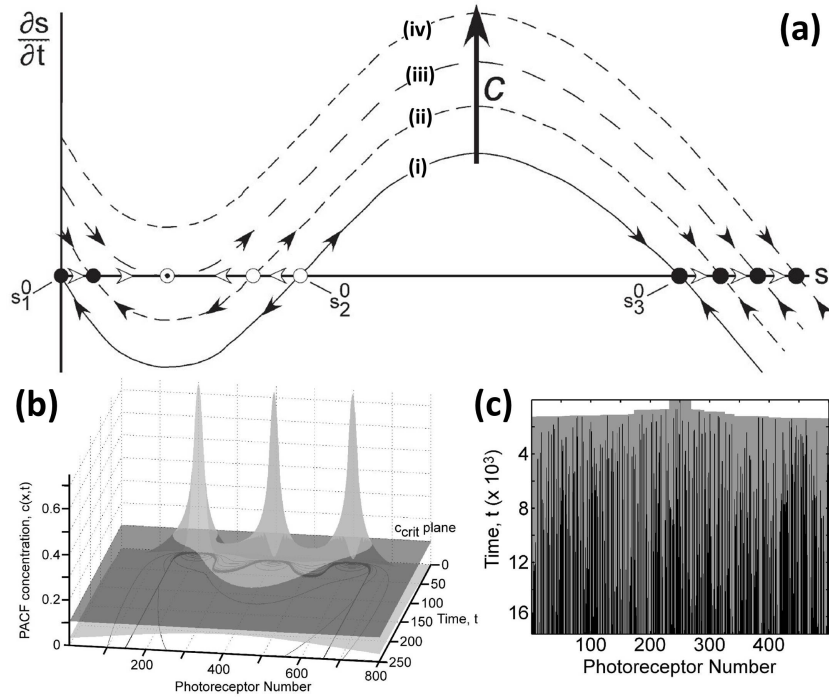


Figure 8: Burns et al.'s toxic substance model of RP. (a) graph showing how the time rate of change of pre-apoptotic factor concentration, $\partial s/\partial t$, evolves with increasing PACF (photoreceptor apoptosis commitment factor), c , concentration. When $c = 0$ (i), the system has three steady-states; two stable steady-states, s_1^0 (corresponding to the MSS) and s_3^0 (corresponding to the apoptosis commitment state), separated by an unstable steady-state, s_2^0 . As c increases past c_{crit} (iii), s_1^0 and s_2^0 meet and annihilate, such that only s_3^0 remains for $c > c_{crit}$ (iv). When the system becomes irreversibly trapped by s_3^0 's basin of attraction, it is considered to be committed to apoptosis. (b) graph showing the recruitment of photoreceptors to apoptosis, following three bursts of PACF release, at close points in space and time. PACF is released at $(x, t) = (20, 0)$, $(40, 10)$ and $(60, 5)$. The light grey surface shows the evolution of PACF concentration in space and time, whilst the dark grey surface is the $c(x, t) = c_{crit}$ plane. The black curve on the $c(x, t) = 0$ plane delimits the photoreceptors which have committed to apoptosis. The PACF bursts act synergistically, such that more photoreceptors are recruited to apoptosis than in the case where the bursts are more distantly separated in space and time. (c) stochastic simulation in which photoreceptors in the apoptosis commitment state undergo apoptosis after a time drawn from an exponential distribution. Upon undergoing apoptosis, a photoreceptor releases a burst of PACF, committing neighbouring cells to apoptosis. Grey regions represent photoreceptors committed to apoptosis and black regions represent photoreceptors which have undergone apoptosis. The recruitment cascade is initiated by a single PACF burst at $(x, t) = (250, 0)$. The results demonstrate a patchy loss of photoreceptors, similar to that which is often seen in the early stages of RP. Figures reproduced, with permission (and modification in (a)), from Burns et al. [18].

1203 Numerical solution and mathematical analysis of the steady¹²²³
 1204 state 1D problem without capillary loss reveals the condition¹²²⁴
 1205 under which a patch (corresponding to an annulus in 2D) of¹²²⁵
 1206 photoreceptor degeneration will spread or remain stable. It is¹²²⁶
 1207 found that the retina may be divided into a series of 5 concentri¹²²⁷
 1208 stability regions, centred on the fovea (see Figure 9(a)). Starting¹²²⁸
 1209 from the centre of the retina these regions are: the central un¹²²⁹
 1210 stable region, the near-central stable region, the para/perifoveal¹²³⁰
 1211 unstable region, the mid-peripheral stable region and the pe¹²³¹
 1212 ripheral unstable region. Wide patches (with width greater than¹²³²
 1213 about one-hundredth of the width of the domain) remain sta¹²³³
 1214 ble to small losses of photoreceptors, provided both boundarie¹²³⁴
 1215 lie within a stable region, and will expand otherwise. There¹²³⁵
 1216 fore, provided a patch can be classified as wide, its stability¹²³⁶
 1217 properties do not depend upon its width, only the position of its¹²³⁷
 1218 boundaries. Narrow patches (with width less than about one¹²³⁸
 1219 hundredth of the width of the domain, that is, less than about¹²³⁹
 1220 40 photoreceptors across) are stable within the 'stable' regions¹²⁴⁰
 1221 and are also stable within 'unstable' regions, provided they are¹²⁴¹
 1222 sufficiently narrow. ¹²⁴²

Simulations of the dynamic (time-dependent) 1D problem without capillary loss and with an initial patch of photoreceptor loss, together with mathematical analysis, reveal that the *wave speed* of photoreceptor degeneration is a decreasing function of the photoreceptor density local to the degenerating wavefront. This prediction awaits experimental/clinical confirmation.

Numerical solution and mathematical analysis of the steady-state 1D problem including capillary loss, reveals the counter-intuitive result that a patch of capillary loss must be essentially coincident with a patch of photoreceptor loss in order to stabilise it, in those cases where it would otherwise be unstable (given the assumption that the capillary loss does not extend beyond the degenerate photoreceptor patch). This is surprising, as it would have been natural to assume that a substantial region of capillary loss, within a patch of photoreceptor loss, would be sufficient to prevent further hyperoxia-driven photoreceptor degeneration. However, the above result suggests that this is not the case. This prediction could be tested experimentally in an animal model by using a laser to ablate the choroid within a patch of photoreceptor loss and also suggests a potential treat-

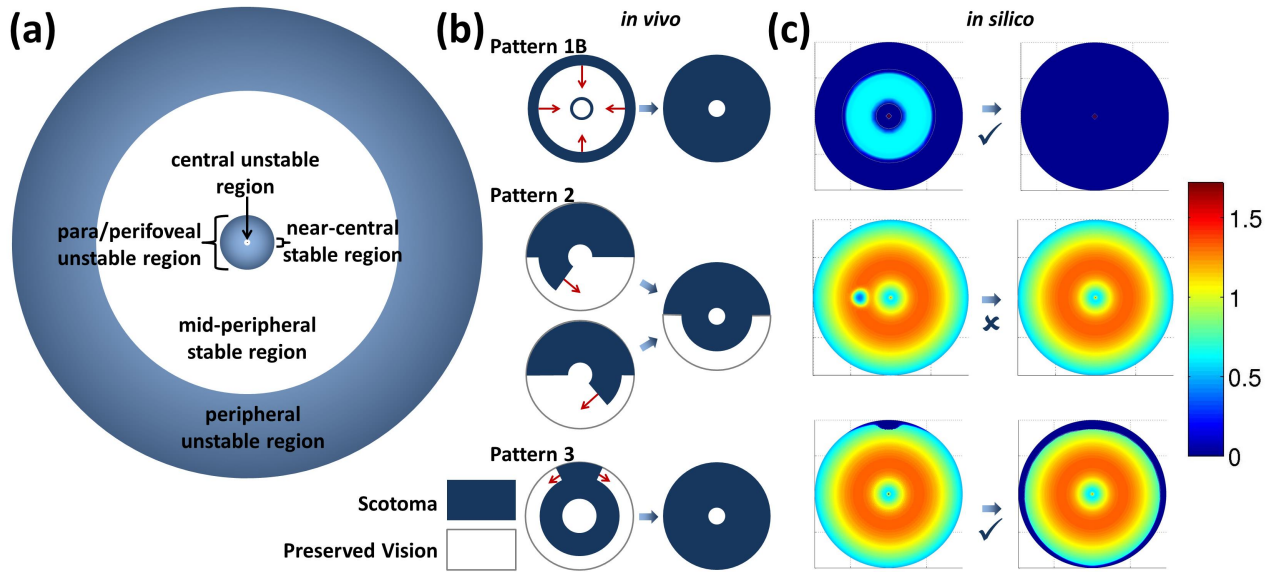


Figure 9: Roberts's oxygen toxicity model of RP. (a) diagram to show the arrangement of stable and unstable regions within the retina. (b) diagrams to show some of the *in vivo* patterns of visual field loss. Scotomas (blind spots) are shaded and areas of preserved vision are shown in white. (c) *in silico* results. Graphs show the photoreceptor density at earlier (left) and later (right) stages (the calibration of the heat map is given by the colour bar on the right, where 1 corresponds to 1.11×10^5 photoreceptors/mm²). The problem is solved on a spherical surface and projected onto the *x-y* plane for visualisation. Pattern 1B and the later stage of pattern 3 are replicated; however, pattern 2 cannot be replicated (in the example shown, a partially degenerate disc recovers fully, in the sense of regaining vitality), the retina being resistant to the spread of photoreceptor degeneration in the mid-peripheral stable region. Figures reproduced, with permission and modifications, from Roberts [92].

ment strategy to arrest the progression of the disease in humans

Dynamic simulations including capillary loss in 1D demonstrate that capillary loss may prevent, halt, delay or partially reverse (in the sense of restoring photoreceptor vitality, given that new photoreceptors cannot be generated) photoreceptor loss. Further experimental work is required to quantify the rate of CC degeneration and hence to determine its effect on photoreceptor degeneration.

The second set of models extends the previous models to 2D, spanning the region between the centre of the fovea and the ora serrata, whilst assuming that the capillary density remains constant. Simulations of the dynamic 2D problem demonstrate the *spatio-temporal patterns* of degeneration that the oxygen toxicity hypothesis can give rise to. In addition to the initial removal of annulus and disc shaped patches of photoreceptors the hyperoxia-independent *mutation-induced* degeneration of either rods and/or cones is also included in some simulations to represent the rod-cone, cone-rod and simultaneous forms of RP. The patterns formed are compared with those classified by Grover et al. [48] in their study of visual loss in RP patients. Grover et al. identified three characteristic patterns or visual field loss: *pattern 1* involves concentric loss of visual field sometimes accompanied by a perifoveal or parafoveal ring scotoma (blind spot); *pattern 2* begins with a nasal or temporal restriction, out from which an arcuate (bow shaped) scotoma winds through the mid-periphery; lastly, *pattern 3* starts with mid-peripheral ring scotoma, which expands either temporally or inferiorly, leaving a U- or n-shaped peripheral visual field the arms of which retract until peripheral vision is lost (see Fig-

ure 9(b)). In all cases, central vision is best preserved, though it is eventually lost unless preceded by patient mortality.

It is found that mutation-induced rod degeneration results in pattern 1 degeneration, including a para/perifoveal ring scotoma (see Figure 9(c)(top)), whilst patch loss in, or overlapping, the para/perifoveal region may also spread to form a para/perifoveal ring scotoma. Patch loss near the ora serrata spreads around the periphery of the retina, mimicking the latter stage of pattern 3 degeneration (see Figure 9(c)(bottom)). Mutation-induced cone loss results in degeneration of the central retina and may in some cases also result in degeneration of the peripheral unstable region. These results are consistent with the cone-rod dystrophy degeneration patterns described by Hamel [50]. It is not possible, with this model, to stimulate preferential loss from the middle of the mid-periphery associated with the intermediate stage of pattern 2 and the initial stage of pattern 3 (see Figure 9(c)(middle)). By isolating the oxygen toxicity mechanism, in a way that would not have been possible experimentally, these models highlight the strengths and weaknesses of this hypothesis. The replication of patterns seen *in vivo* demonstrates the sufficiency (though not the necessity) of this mechanism to generate certain patterns of degeneration, whilst the failure to replicate other patterns indicates that other mechanisms are likely to be at play here. This provides a useful insight for the development of future treatment strategies.

Both 1D and 2D models predict that treatment with *antioxidants* and/or *trophic factors* could prevent, halt, delay or partially reverse (in the sense of restoring photoreceptor vitality) photoreceptor loss, depending upon the strength and timing of

1301 the treatment. Since the analysis and simulations indicate that¹³⁵⁷
1302 the para/perifoveal and peripheral unstable regions are the most¹³⁵⁸
1303 susceptible to hyperoxic degeneration, this suggests that, if pos¹³⁵⁹
1304 sible, treatment should preferentially target these regions. ¹³⁶⁰

1305 A natural way to extend this modelling work would be to¹³⁶¹
1306 adapt the modelling framework, with its incorporation of the¹³⁶²
1307 distribution of rods and cones, to consider the dynamics of dis¹³⁶³
1308 ease progression under the trophic factor and toxic substanc¹³⁶⁴
1309 hypotheses. These models could perhaps explain the other ob¹³⁶⁵
1310 served patterns of photoreceptor loss in RP. The latter hypoth¹³⁶⁶
1311 esis has particular potential to explain the preferential loss of¹³⁶⁷
1312 photoreceptors from the middle of the mid-periphery seen in¹³⁶⁸
1313 progression patterns 2 and 3, as it is here that the toxin produc¹³⁶⁹
1314 ing rods are most densely packed. This could then be followed¹³⁷⁰
1315 by more comprehensive models which combine the three RP¹³⁷¹
1316 hypotheses. Following sufficient benchmarking, such models¹³⁷²
1317 could be used to inform treatment decisions, parametrising the¹³⁷³
1318 model to make it patient specific. ¹³⁷⁴

1319 Perhaps the most useful data, for informing future mod¹³⁷⁵
1320 elling studies, could be derived from a detailed longitudinal¹³⁷⁶
1321 clinical study, measuring the precise positions of the bound¹³⁷⁷
1322 aries of degenerate photoreceptor, RPE and CC patches, at reg¹³⁷⁸
1323 ular intervals throughout the disease progression, together with¹³⁷⁹
1324 the rod and cone densities across the retina at each stage, in¹³⁸⁰
1325 a range of patients. This could be done using optical coher¹³⁸¹
1326 ence tomography and adaptive optics scanning light ophthal¹³⁸²
1327 moscopy [69, 86]. Combining this with visual field tests, multi¹³⁸³
1328 focal electroretinograms and autofluorescence imaging would¹³⁸⁴
1329 enhance these studies still further [94]. This would yield better¹³⁸⁵
1330 parametrised models, which have the potential to more accu¹³⁸⁶
1331 rately predict the pattern and speed of degeneration. Present¹³⁸⁷
1332 studies tend to focus on the patterns of visual field loss, rather¹³⁸⁸
1333 than changes in the photoreceptor density, making it difficult¹³⁸⁹
1334 to determine precise measurements for the retinal locations af¹³⁹⁰
1335 fected. In addition, the early stages in the disease progression¹³⁹¹
1336 are often not recorded (largely because symptoms tend not to¹³⁹²
1337 manifest until later in life) and the intervals between measure¹³⁹³
1338 ments are too long (it would be helpful if observations could be¹³⁹⁴
1339 made on at least an annual basis). ¹³⁹⁵

1340 5.2. Choroidal Neovascularisation ¹³⁹⁷

1341 *Choroidal neovascularisation* (CNV) is a process which oc¹³⁹⁸
1342 curs during the advanced stage of neovascular (wet) AMD [55]¹³⁹⁹
1343 It involves the growth and spread of the choroid past *Bruch's*¹⁴⁰⁰
1344 *membrane* (BM), which in health forms a barrier between the¹⁴⁰¹
1345 choroid and the RPE, into the retina. The choroidal vessels¹⁴⁰²
1346 penetrating the retina are abnormally permeable and fragile¹⁴⁰³
1347 leading to the build-up of fluid and subsequent damage to the¹⁴⁰⁴
1348 retina. The physiological and biochemical mechanisms under¹⁴⁰⁵
1349 lying CNV are not well understood, whilst present treatment¹⁴⁰⁶
1350 strategies show limited success [29]. ¹⁴⁰⁷

1351 Flower et al. [42] have constructed a model which relates¹⁴⁰⁸
1352 the blood flow in the CNV to that in the underlying CC. The¹⁴⁰⁹
1353 CC is modelled as a (2D) planar porous medium, with a set¹⁴¹⁰
1354 of sparsely distributed inflows and outflows (arranged accord¹⁴¹¹
1355 ing to the histology of a sample human eye), which supply and¹⁴¹²
1356 drain blood from deeper within the choroid, whilst the CC is¹⁴¹³

connected to the CNV via capillary-like vessels. The model predicts that reducing the blood flow in an arteriole/venule, feeding/draining the CC, by as little as 50% could be sufficient to significantly reduce or halt blood flow in an overlying CNV, whose penetrating vessels neighbour the arteriole/venule.

The model has clear implications for potential treatment strategies. Flower et al. [42] suggest that it may be better to target the underlying choroid, rather than destroying the CNV, which often results in recurrence. At present, treatment only targets arterioles, whereas the model suggests that ablating venules could be just as effective. If the model could be tailored to individual patients, then it could potentially be used to determine which arterioles and venules to target, optimising treatment.

Shirinifard et al. [101] have developed a 3D computational model of the choroid and outer retina in which they investigate the role played by *adhesion* in CNV progression. The model is of the *cellular Potts* type, where each model 'cell' is composed of a set of (simply) connected points on a pre-defined lattice. The model 'cells' may either represent biological cells, parts of cells or fluid-containing regions, their positions being updated stochastically over time, subject to energy (e.g. adhesion energies) and other constraints. The model accounts for vascular cells (of the CC), stalk cells (of the CNV), tip cells, RPE cells, photoreceptor OS cell parts, photoreceptor IS cell parts, BM, medium (which fills the spaces unoccupied by cells or BM), oxygen, VEGF and matrix metalloproteinases (MMP).

Each simulation begins either with or without a single *tip cell* (an endothelial cell which leads other endothelial cells upon activation of sprouting angiogenesis), which degrades the BM via the secretion of MMP, allowing it to penetrate the retina. In each case, the simulation time covers a year's disease progression, the first three months of which are regarded as the *early phase* and the last three months of which are denoted the *late phase*.

In both the early and late phases, one of three patterns of vascularisation may occur: *type 1* (sub-RPE) CNV, with a vascular layer between BM and the RPE; *type 2* (sub-retinal) CNV, with a vascular layer between the RPE and the photoreceptors; and *type 3* (combined pattern) CNV, which combines both of the above vascular layers. The model accounts for the adhesion between RPE cells and BM (RPE-BM), between neighbouring RPE cells (RPE-RPE) and between RPE cells and photoreceptor OSs (RPE-POS, see Figure 10(a)). All three pairings involve *labile adhesion* (without junctional structures), whilst the first two also involve *plastic coupling* (with junctional structures). The combination of these two types of adhesion is known as *junctional adhesion*. This gives rise to five adhesion parameters, corresponding to each of the adhesion types between each sort of structure. By varying these parameters, the effects of adhesion failure upon disease progression can be determined (see Figure 10(b)).

A total of six scenarios are observed, as judged by the pattern of vascularisation at the early and late phases: stable type 1 (early and late type 1), early type 1 to late type 2 (see Figures 10(c) and (d)), early type 1 to late type 3, stable type 2 (early and late type 2), early type 2 to late type 3, and stable type 3 (early and late type 3). It is found that the combination of the

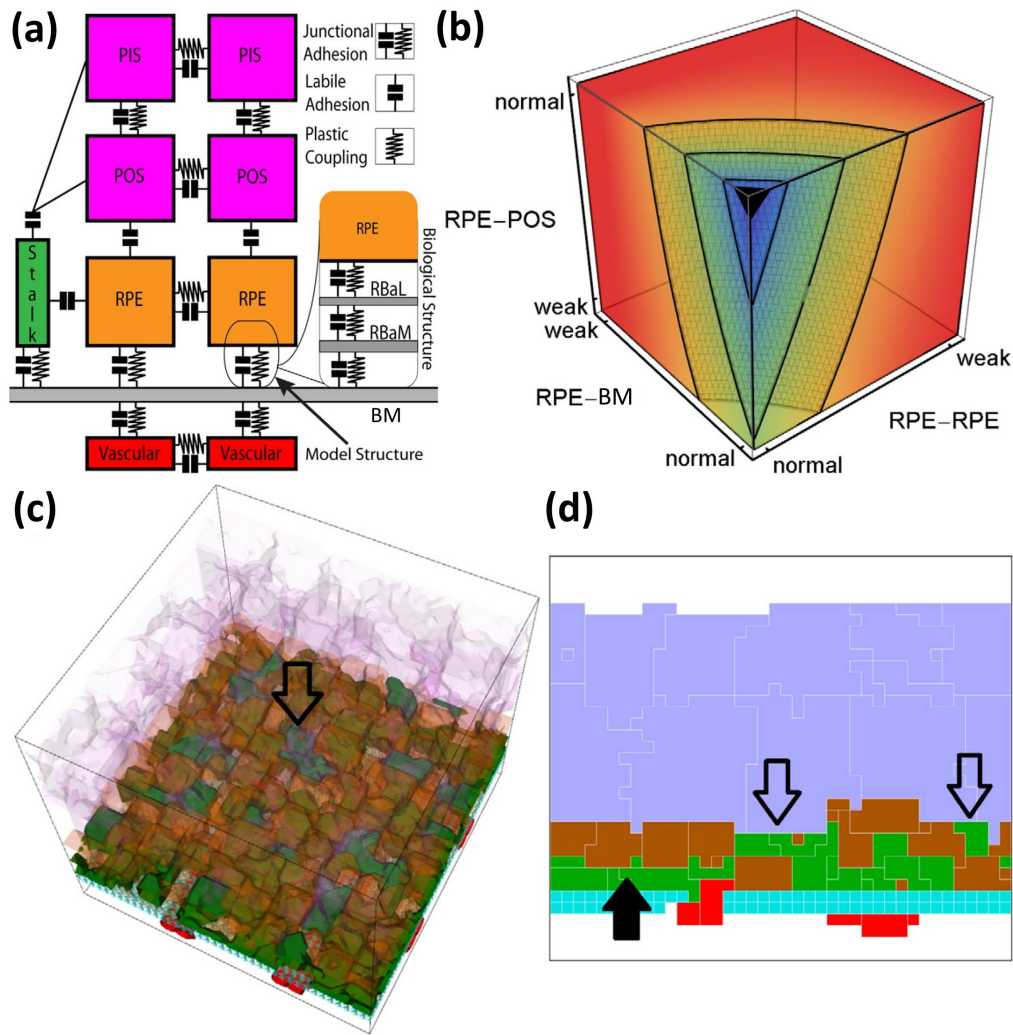


Figure 10: Shirinifard et al.'s model of CNV. (a) diagram showing the adhesive coupling between retinal components. Plastic coupling involves junctional structures, whilst labile adhesion does not. Junctional adhesion is the combination of plastic coupling and labile adhesion. (b) sensitivity analysis showing the dependence of the CNV initiation probability upon the strength of the RPE-POS, RPE-BM and RPE-RPE adhesive coupling. Red corresponds to a probability of 1 and purple to a probability of 0. The black region (top-front corner) demarcates the locus of normal adhesion. The isosurfaces correspond to initiation probabilities of 0.25, 0.5 and 0.75, from front to back. (c) and (d) snapshots from a simulation showing type 1 (sub-RPE) to type 2 (sub-retinal) CNV progression. PIS and POS are light purple, RPE is brown, stalk cells are green, vascular (CC) cells are red and BM is light blue. (c) 3D snapshot at month 6. The open arrow indicates a location at which stalk cells have migrated into the sub-retinal space. (d) 2D snapshot at month 12. The black arrow marks the sub-RPE capillary network, whilst the open arrows mark the sub-retinal capillary network. PIS: photoreceptor inner segment, POS: photoreceptor outer segment, RPE: retinal pigment epithelium, BM: Bruch's membrane, RBaL: basal lamina of the RPE, RBaM: basement membrane of the RPE, CC: choriocapillaris. Figures reproduced, with permission (and modifications in (a) and (b)), from Shirinifard et al. [101].

1414 presence of a tip cell and the occurrence of adhesion failures^{S426}
 1415 are both necessary and sufficient for CNV to initiate, and that⁴²⁷
 1416 severe impairment of any one of the three adhesion pairings can⁴²⁸
 1417 independently induce CNV. In particular, reduced RPE-BM ad⁴²⁹
 1418 hesion results in early type 1, reduced RPE-RPE or RPE-POS⁴³⁰
 1419 adhesion results in early type 2, and simultaneous reduction of⁴³¹
 1420 RPE-RPE and RPE-BM results in either early type 1 or early⁴³²
 1421 type 2, which may often progress to late type 3. Simulations⁴³³
 1422 also reveal that the plastic coupling strengths have a relatively⁴³⁴
 1423 minor effect on the ability of the retina to resist CNV, with labile⁴³⁵
 1424 adhesion playing the most important role. ¹⁴³⁶

1425 Many previous studies have suggested that CNV results ei⁴³⁷

ther from the overexpression of VEGF or holes in BM [101]. Simulations demonstrate that overexpression of VEGF increases the probability of CNV initiation, but that the early and late vascular patterns do not change, whilst holes in BM are insufficient to initiate CNV when all the adhesions are normal. In addition, neither the threshold for RPE hypoxia, nor RPE hypoxic signalling, affects the results. Thus, the model provides important insights into CNV.

Simulations show good agreement with experimental and clinical data, though there are some discrepancies. For example, the type 1 to type 2 progression has not been observed clinically. It may be that this progression does occur, but that it is

1438 difficult to detect, requiring more frequent observations over a
1439 longer period of time [101].

1440 Future modelling work could include blood flow and its ef-
1441 fect on capillary development in a similar way to McDougall
1442 et al. [77] and Watson et al. [119] (Section 4.1) and perhaps also
1443 blood flow within the CC as in Zouache et al. [131] (Section 3.3)
1444 noting that Shirinifard et al.'s model assumes that oxygen levels
1445 are constant throughout the blood vessels). Additionally, basal
1446 deposits such as hard and soft drusen, together with fibrosis (the
1447 formation of extracellular matrix) could also be included in fu-
1448 ture models [101].

1449 Experimental quantification of the adhesivities between the
1450 cells of the retina and how these change under pathological
1451 conditions would allow more effective validation of the model
1452 together with more clinically accurate predictions. Shirinifard
1453 et al. suggest that these measurements could be made non-invasively
1454 by examining changes in RPE and CC morphology, or changes
1455 in autofluorescence due to lipid accumulation.

1456 In time, and following extensive trials, this model, or a re-
1457 fined version thereof, could become a useful clinical tool, al-
1458 lowing for more accurate determination of each patient's pathol-
1459 ogy and, hence, inform the selection of the most appropriate
1460 treatment strategy (i.e. personalised medicine). Further, Shirini-
1461 fard et al. suggest that the model could be continuously im-
1462 proved using data from each clinical or experimental case to
1463 which it is applied (e.g. using machine learning).

1464 6. Perspective and Future Directions

1465 The *mathematical* and *computational models* discussed in
1466 this paper have uncovered a wealth of insights into retinal phys-
1467 iology and biochemistry, across a range of scenarios, spanning
1468 the healthy, developmental and diseased states. Whilst models
1469 are developed with a particular state in mind, it is often the case
1470 that they may be adapted to examine one or both of the other
1471 two states. In particular, many of the models of the healthy and
1472 developing retina can be used to explore pathological scenarios.

1473 In the *healthy state*, theoretical models have enabled us to
1474 explain the retinal oxygen distribution in terms of the varia-
1475 tion in oxygen demand between different retinal layers, allow-
1476 ing the identification of the chief oxygen consumers and an
1477 investigation of how consumption varies between light adap-
1478 tation and dark adaptation. Further, it has been demonstrated
1479 that the protein neuroglobin may play an important role in the
1480 prevention of hypoxia within the retina, through its ability to
1481 transport oxygen from regions where it is rich to those where
1482 it is poor, its oxygen affinity being near-optimal for this pro-
1483 cess. Modelling of blood flow within the choriocapillaris has
1484 demonstrated the effect of lobule geometry upon the flow prop-
1485 erties within each lobule, suggesting how blood flow will vary
1486 across the eye with geographical variation in lobule geome-
1487 try. This may also be a factor in the spatially heterogeneous
1488 progression of diseases such as retinitis pigmentosa (RP) and
1489 age-related macular degeneration (AMD). Lastly, it has been
1490 demonstrated that the diurnal variation in photoreceptor outer
1491 segment (OS) length may be regulated by the oxygen and phos-
1492 phocreatine shuttle-derived ATP landscape within the photore-

ceptor, but that neither of these factors in isolation is sufficient
to explain this variation. It is shown that inefficiencies in mi-
tochondrial function or OS energy utilisation give rise to OS
shortening, a phenomenon observed in many retinal diseases
such as RP and AMD.

In the *developing state*, mathematical and computational
models of retinal angiogenesis have captured the *in vivo* dy-
namics of retinal vascular plexus formation with a remarkable
degree of accuracy. The importance of perfusion, plexus re-
modelling, and convected and conducted stimuli for the devel-
opment of highly structured vascular trees is demonstrated. The
model is also used to predict the effect of various parameter val-
ues and model components upon development. For example, if
the input arterial haematocrit is increased, or the rate of tissue
oxygen consumption is decreased, hyperoxia develops, leading
to the formation of large capillary-free zones. The former case
is equivalent to retinopathy of prematurity and the latter to oxy-
gen induced retinopathy, producing similar predicted outcomes
to those seen in these conditions.

In the *diseased state*, mathematical and computational mod-
els have been used to investigate RP and choroidal neovascular-
isation (CNV). In RP, models have explored the trophic factor,
toxic substance and oxygen toxicity hypotheses. Trophic factor
models demonstrate the rhythmic shedding and renewal of pho-
toreceptors seen *in vivo*. The photoreceptor (cone, normal rod
and mutant rod) shedding to renewal ratios and trophic factor
carrying capacity are found to be key in determining the ad-
vancement of RP through various disease states, providing po-
tential clues to treatment. The toxic substance model is able
to replicate the exponential decline in photoreceptor number
seen in experiments, together with the patchy photoreceptor
loss seen in the early stages of RP. The oxygen toxicity model
suggests that this mechanism is sufficient to explain some, but
not all of the *in vivo* spatio-temporal patterns of degeneration,
demonstrating the strengths and weaknesses of this hypothesis.
Lastly, the CNV model demonstrates that adhesion failures be-
tween outer retinal components, together with the presence of
a tip cell, are necessary and sufficient conditions for CNV to
initiate.

The above studies demonstrate the power of mathematical
and computational modelling in investigating the structure and
function of the retina. Despite the advances which have been
made, theoretical modelling has yet to achieve its full potential
in this area, current work representing merely the tip of the ice-
berg, given the possibilities which have yet to be explored. In
the healthy state, much work remains to be done in modelling
processes such as the visual cycle, photoreceptor-RPE interac-
tions, pre-processing of visual information by the retina and
aging of the retina. In development, there is scope for exten-
sive work targeted at understanding how the complex layered
structure of the retina arises, including retinal mosaic forma-
tion, together with the establishment of the full 3D structure of
the retinal capillary layers. Many retinal diseases start to take
effect during the developmental stage, therefore extensive mod-
elling of retinal development will be required in order to fully
understand these pathologies. Substantial further work remains
for RP and AMD, whilst other disease states such as diabetic

retinopathy, retinopathy of prematurity and retinoblastoma are largely untouched. Ultimately, the aim would be to produce a collection of validated models, individually detailing an important aspect of the retina, which can subsequently be coupled, as required, to enable retinal modelling that can encompass development, health and the full range of disease states. These could then be used as clinical tools, to inform personalised treatment strategies.

In order to achieve these aims, greater attention to this area is required from the mathematical and computational modelling communities, together with an increase in ophthalmic clinicians and experimentalists ready to work with theoreticians to parametrise and validate their models and to test model predictions (thus completing the experiment/modelling cycle, see Figure 1). At present, whilst a lot of data are available on the retina, many of the parameters which are key to forming accurate models have yet to be precisely measured, despite advances in experimental, diagnostic and imaging techniques rendering these measurements tractable. As experimental/theoretical collaborations increase, so too will the insights which can be obtained into the retina, making possible discoveries which neither set of disciplines could have achieved on its own.

Acknowledgements

We gratefully acknowledge the Engineering and Physical Sciences Research Council (EPSRC) in the UK for funding through a studentship at the Systems Biology programme of the University of Oxford's Doctoral Training Centre P.A.R.

[1] Abrámoff, M. D., Mullins, R. F., Lee, K., Hoffmann, J. M., Sonka, M., Critser, D. B., Stasheff, S. F., Stone, E. M., 2013. Human photoreceptor outer segments shorten during light adaptation. *Invest. Ophthalmol. Vis. Sci.* 54 (5), 3721–3728.

[2] Ames, B. N., Shigenaga, M. K., Hagen, T. M., 1993. Oxidants, antioxidants, and the degenerative diseases of aging. *Proc. Natl. Acad. Sci.* 90 (17), 7915–7922.

[3] Ames, B. N., Shigenaga, M. K., Hagen, T. M., 1995. Mitochondrial decay in aging. *Biochim. Biophys. Acta.* 1271 (1), 165–170.

[4] Anderson, B., 1968. Ocular effects of changes in oxygen and carbon dioxide tension. *Trans. Am. Ophthalmol. Soc.* 66, 423–474.

[5] Anderson, B., Saltzman, H. A., 1964. Retinal oxygen utilization measured by hyperbaric blackout. *Arch. Ophthalmol.* 72 (6), 792–795.

[6] Aubert, M., Chaplain, M. A. J., McDougall, S. R., Devlin, A., Mitchell, C. A., 2011. A continuum mathematical model of the developing murine retinal vasculature. *Bull. Math. Biol.* 73, 2430–2451.

[7] Band, L. R., Hall, C. L., Richardson, G., Jensen, O. E., Siggers, J. H., Foss, A. J. E., 2009. Intracellular flow in optic nerve axons: A mechanism for cell death in glaucoma. *Invest. Ophthalmol. Vis. Sci.* 50 (8), 3750–3758.

[8] Barton, A., Fendrik, A. J., 2015. Retinogenesis: Stochasticity and the competency model. *J. Theor. Biol.* 373 (0), 73–81.

[9] Bassi, C. J., Powers, M. K., 1990. Shedding of rod outer segments is light-driven in goldfish. *Invest. Ophthalmol. Vis. Sci.* 31 (11), 2314–2319.

[10] Braun, R. D., Linsenmeier, R. A., Goldstick, T. K., 1995. Oxygen consumption in the inner and outer retina of the cat. *Invest. Ophthalmol. Vis. Sci.* 36 (3), 542–554.

[11] Braun, R. J., 2012. Dynamics of the tear film. *Annu. Rev. Fluid Mech.* 44 (1), 267–297.

[12] Braun, R. J., King-Smith, P. E., Begley, C. G., Li, L., Gewecke, N. R., 2015. Dynamics and function of the tear film in relation to the blink cycle. *Prog. Retin. Eye. Res.* 45, 132–164.

[13] Brunori, M., Vallone, B., 2007. Neuroglobin, seven years after. *Cell. Mol. Life Sci.* 64, 1259–1268.

[14] Burd, H. J., Regueiro, R. A., 2015. Finite element implementation of a multiscale model of the human lens capsule. *Biomech. Model Mechanobiol.*, 1–16.

[15] Burmester, T., Hankeln, T., 2004. Neuroglobin: A respiratory protein of the nervous system. *News Physiol. Sci.* 19 (3), 110–113.

[16] Burmester, T., Hankeln, T., 2009. What is the function of neuroglobin? *J. Exp. Biol.* 212 (10), 1423–1428.

[17] Burmester, T., Weich, B., Reinhardt, S., Hankeln, T., 2000. A vertebrate globin expressed in the brain. *Nature* 407 (6803), 520–523.

[18] Burns, J., Clarke, G., Lumsden, C. J., 2002. Photoreceptor death: Spatiotemporal patterns arising from one-hit death kinetics and a diffusible cell death factor. *Bull. Math. Biol.* 64, 1117–1145.

[19] Camacho, E., Rand, R., Howland, H., 2004. Dynamics of two van der Pol oscillators coupled via a bath. *Int. J. Solids Struct.* 41 (8), 2133–2143.

[20] Camacho, E. T., Colón Vélez, M. A., Hernández, D. J., Bernier, U. R., van Laarhoven, J., Wirkus, S., 2010. A mathematical model for photoreceptor interactions. *J. Theor. Biol.* 267 (4), 638–646.

[21] Camacho, E. T., Melara, L. A., Villalobos, M. C., Wirkus, S., 2014. Optimal control in the treatment of retinitis pigmentosa. *Bull. Math. Biol.* 76 (2), 292–313.

[22] Camacho, E. T., Wirkus, S., 2013. Tracing the progression of retinitis pigmentosa via photoreceptor interactions. *J. Theor. Biol.* 317 (0), 105–118.

[23] Chan, G., Balaratnasingam, C., Yu, P. K., Morgan, W. H., McAllister, I. L., Cringle, S. J., Yu, D.-Y., 2012. Quantitative morphometry of periferoveal capillary networks in the human retina. *Invest. Ophthalmol. Vis. Sci.* 53 (9), 5502–5514.

[24] Cideciyan, A. V., Hood, D. C., Huang, Y., Banin, E., Li, Z.-Y., Stone, E. M., Milam, A. H., Jacobson, S. G., 1998. Disease sequence from mutant rhodopsin allele to rod and cone photoreceptor degeneration in man. *Proc. Natl. Acad. Sci.* 95 (12), 7103–7108.

[25] Clarke, G., Collins, R. A., Leavitt, B. R., Andrews, D. F., Hayden, M. R., Lumsden, C. J., McInnes, R. R., 2000. A one-hit model of cell death in inherited neuronal degenerations. *Nature* 406, 195–199.

[26] Clarke, G., Lumsden, C. J., 2005. Heterogeneous cellular environments modulate one-hit neuronal death kinetics. *Brain Res. Bull.* 65 (1), 59–67.

[27] Clarke, G., Lumsden, C. J., 2005. Scale-free neurodegeneration: cellular heterogeneity and the stretched exponential kinetics of cell death. *J. Theor. Biol.* 233 (4), 515–525.

[28] Clarke, G., Lumsden, C. J., McInnes, R. R., 2001. Inherited neurodegenerative diseases: the one-hit model of neurodegeneration. *Hum. Mol. Genet.* 10 (20), 2269–2275.

[29] Coleman, H. R., Chan, C. C., Ferris III, F. L., Chew, E. Y., 2008. Age-related macular degeneration. *Lancet* 372 (9652), 1835–1845.

[30] Colón Vélez, M. A., Hernández, D. J., Bernier, U. R., van Laarhoven, J., Camacho, E. T., 2003. Mathematical models for photoreceptor interactions. Tech. rep., Cornell University, Department of Biological Statistics and Computational Biology.

[31] Connor, A. J., Nowak, R. P., Lorenzon, E., Thomas, M., Herting, F., Høert, S., Quaiser, T., Shochat, E., Pitt-Francis, J., Cooper, J., Maini, P. K., Byrne, H. M., 2015. An integrated approach to quantitative modelling in angiogenesis research. *J. R. Soc. Interface* 12 (110).

[32] Cringle, S., Yu, D. Y., Alder, V., Su, E. N., Yu, P., 1996. Oxygen consumption in the avascular guinea pig retina. *Am. J. Physiol. Heart. Circ. Physiol.* 271 (3), H1162–H1165.

[33] Cringle, S. J., Yu, D. Y., 2002. A multi-layer model of retinal oxygen supply and consumption helps explain the muted rise in inner retinal PO₂ during systemic hyperoxia. *Comp. Biochem. Physiol.* 132 (1), 61–66.

[34] de Vries, G., Hillen, T., Lewis, M. A., Müller, J., Schönlisch, B., 2006. A Course in Mathematical Biology: Quantitative Modeling with Mathematical and Computational Methods. Monographs on Mathematical Modeling and Computation. SIAM publishing.

[35] Dollery, C. T., Bulpitt, C. J., Kohner, E. M., 1969. Oxygen supply to the retina from the retinal and choroidal circulations at normal and increased arterial oxygen tensions. *Invest. Ophthalmol. Vis. Sci.* 8 (6), 588–594.

[36] Eglen, S. J., 2006. Development of regular cellular spacing in the retina: theoretical models. *Math. Med. Biol.* 23 (2), 79–99.

[37] Eglen, S. J., 2012. Cellular spacing: Analysis and modelling of retinal mosaics. In: Le Novère, N. (Ed.), *Computational Systems Neurobiol-*

- ogy. Springer, Ch. 12, pp. 365–385. 1754
- [38] Ethier, C. R., Johnson, M., Ruberti, J., 2004. Ocular biomechanics and 1755
biotransport. *Annu. Rev. Biomed. Eng.* 6 (1), 249–273. 1756
- [39] Fago, A., Hundahl, C., Malte, H., Weber, R. E., 2004b. Functional prop+757
erties of neuroglobin and cytoglobin. insights into the ancestral physio+758
logical roles of globins. *IUBMB Life* 56 (11–12), 689–696. 1759
- [40] Filas, B. A., Shui, Y. B., Beebe, D. C., 2013. Computational model for+760
oxygen transport and consumption in human vitreous. *Invest. Ophthal+761
mol. Vis. Sci.* 54 (10), 6549–6559. 1762
- [41] Fintz, A. C., Audo, I., Hicks, D., Mohand-Saïd, S., Lèveillard, T., Sahel+763
J., 2003. Partial characterization of retina-derived cone neuroprotection+764
in two culture models of photoreceptor degeneration. *Invest. Ophthal+765
mol. Vis. Sci.* 44 (2), 818–825. 1766
- [42] Flower, R. W., von Kerczek, C., Zhu, L., Ernest, A., Eggleton, C.,+767
Topoleski, L. D. T., 2001. Theoretical investigation of the role of chori+768
ocapillaris blood flow in treatment of subfoveal choroidal neovascular+769
ization associated with age-related macular degeneration. *Am. J. Oph+770
thalmol.* 132 (1), 85–93. 1771
- [43] Friedland, A. B., 1978. A mathematical model of transmural transport+772
of oxygen to the retina. *Bull. Math. Biol.* 40 (6), 823–837. 1773
- [44] Friedman, E., Smith, T. R., Kuwabara, T., 1963. Senile choroidal vascu+774
lar patterns and drusen. *Arch. Ophthalmol.* 69 (2), 220–230. 1775
- [45] Ganesan, P., He, S., Xu, H., 2010. Analysis of retinal circulation using+776
an image-based network model of retinal vasculature. *Microvasc. Res*+777
80 (1), 99–109. 1778
- [46] Ganesan, P., He, S., Xu, H., 2010. Development of an image-based net+779
work model of retinal vasculature. *Ann. Biomed. Eng.* 38, 1566–1585. 1780
- [47] García-Ayuso, D., Ortín-Martínez, A., Jiménez-López, M., Galindo+781
Romero, C., Cuenca, N., Pinilla, I., Vidal-Sanz, M., Agudo-Barrusio+782
M., Villegas-Pérez, M. P., 2013. Changes in the photoreceptor mosaï+783
of P23H-1 rats during retinal degeneration: Implications for rod-cone+784
dependent survival. *Invest. Ophthalmol. Vis. Sci.* 54 (8), 5888–5900. 1785
- [48] Grover, S., Fishman, G. A., Brown Jr, J., 1998. Patterns of visual+786
field progression in patients with retinitis pigmentosa. *Ophthalmology*+787
105 (6), 1069–1075. 1788
- [49] Hamel, C., 2006. Retinitis pigmentosa. *Orphanet. J. Rare Dis.* 1 (1), 40+789
- [50] Hamel, C., 2007. Cone rod dystrophies. *Orphanet. J. Rare Dis.* 2 (1), 7+790
- [51] Hartong, D. T., Berson, E. L., Dryja, T. P., 2006. Retinitis pigmentosa+791
Lancet 368 (9549), 1795–1809. 1792
- [52] Haugh, L., Linsenmeier, R., Goldstick, T., 1990. Mathematical models+793
of the spatial distribution of retinal oxygen tension and consumption+794
including changes upon illumination. *Ann. Biomed. Eng.* 18, 19–36. 1795
- [53] Howison, S., 2005. *Practical Applied Mathematics: Modelling, Anal+796
ysis, Approximation.* Cambridge Texts in Applied Mathematics. Cam+797
bridge University Press. 1798
- [54] Jackson, T., Zheng, X., 2010. A cell-based model of endothelial cell mi+799
gration, proliferation and maturation during corneal angiogenesis. *Bull*+800
Math. Biol. 72, 830–868. 1801
- [55] Jager, R. D., Mieler, W. F., Miller, J. W., 2008. Age-related macular+802
degeneration. *N. Engl. J. Med.* 358 (24), 2606–2617. 1803
- [56] Ji, Y., Zhu, C. L., Grzywacz, N. M., Lee, E. J., 2012. Rearrangement of+804
the cone mosaic in the retina of the rat model of retinitis pigmentosa. *J*+805
Comp. Neurol. 520 (4), 874–888. 1806
- [57] Jiann, L. Y., Ismail, Z., Shafie, S., Fitt, A., 2015. Numerical computa+807
tional of fluid flow through a detached retina. *AIP Conference Proceed*+808
ings 1643 (1), 642–648. 1809
- [58] Jiao, Y., Lau, T., Hatzikirou, H., Meyer-Hermann, M., Corbo, J. C.+810
Torquato, S., 2014. Avian photoreceptor patterns represent a disordered+811
hyperuniform solution to a multiscale packing problem. *Phys. Rev. E* 89+812
022721. 1813
- [59] Keener, J., Sneyd, J., 2009. *Mathematical Physiology I: Cellular Physi*+814
ology, 2nd Edition. Interdisciplinary Applied Mathematics. Springer. 1815
- [60] Keener, J., Sneyd, J., 2009. *Mathematical Physiology II: Systems Physi*+816
ology, 2nd Edition. Interdisciplinary Applied Mathematics. Springer. 1817
- [61] King-Smith, P. E., Nichols, J. J., Nichols, K. K., Fink, B. A., Braum+818
R. J., 2008. Contributions of evaporation and other mechanisms to tear+819
film thinning and break-up. *Optometry & Vision Science* 85 (8), 623+820
630. 1821
- [62] Kohen, R., Nyska, A., 2002. Invited review: Oxidation of biological+822
systems: Oxidative stress phenomena, antioxidants, redox reactions, and+823
methods for their quantification. *Toxicol. Pathol.* 30 (6), 620–650. 1824
- [63] Kranz, K., Paquet-Durand, F., Weiler, R., Janssen-Bienhold, U., Dedek, 1825
K., 2013. Testing for a gap junction-mediated bystander effect in re- 1826
tinitis pigmentosa: Secondary cone death is not altered by deletion of 1827
connexin36 from cones. *PLoS One* 8 (2), e57163. 1828
- [64] Kur, J., Newman, E. A., Chan-Ling, T., 2012. Cellular and physiological 1829
mechanisms underlying blood flow regulation in the retina and choroid 1830
in health and disease. *Prog. Retin. Eye. Res.* 31 (5), 377–406. 1831
- [65] Lamb, T. D., Pugh Jr., E. N., 2004. Dark adaptation and the retinoid 1832
cycle of vision. *Prog. Retin. Eye. Res.* 23 (3), 307–380. 1833
- [66] Lee, E. J., Ji, Y., Zhu, C. L., Grzywacz, N. M., 2011. Role of Müller cells 1834
in cone mosaic rearrangement in a rat model of retinitis pigmentosa. *Glia* 1835
59 (7), 1107–1117. 1836
- [67] Lèveillard, T., Mohand-Saïd, S., Lorentz, O., Hicks, D., Fintz, A. C., 1837
Clérin, E., Simonutti, M., Forster, V., Cavusoglu, N., Chalmel, F., Dollé, 1838
P., Poch, O., Lambrou, G., Sahel, J. A., 2004. Identification and charac- 1839
terization of rod-derived cone viability factor. *Nat. Genet.* 36 (7), 755– 1840
759. 1841
- [68] Linsenmeier, R. A., 1986. Effects of light and darkness on oxygen dis- 1842
tribution and consumption in the cat retina. *J. Gen. Physiol.* 88 (4), 521– 1843
542. 1844
- [69] Liu, B. S., Tarima, S., Visotcky, A., Pechauer, A., Cooper, R. F., Land- 1845
sem, L., Wilk, M. A., Godara, P., Makhijani, V., Sulai, Y. N., Syed, 1846
N., Yasumura, G., Garg, A. K., Pennesi, M. E., Lujan, B. J., Dubra, 1847
A., Duncan, J. L., Carroll, J., 2014. The reliability of parafoveal cone 1848
density measurements. *Br. J. Ophthalmol.* 98 (8), 1126–1131. 1849
- [70] Liu, D., Wood, N. B., Witt, N., Hughes, A. D., Thom, S. A., Xu, X. Y., 1850
2009. Computational analysis of oxygen transport in the retinal arterial 1851
network. *Curr. Eye Res.* 34 (11), 945–956. 1852
- [71] Lomasko, T., Clarke, G., Lumsden, C. J., 2007. One-hit stochastic 1853
decline in a mechanochemical model of cytoskeleton-induced neuron 1854
death I: Cell-fate arrival times. *J. Theor. Biol.* 249 (1), 1–17. 1855
- [72] Lomasko, T., Clarke, G., Lumsden, C. J., 2007. One-hit stochastic 1856
decline in a mechanochemical model of cytoskeleton-induced neuron 1857
death II: Transition state metastability. *J. Theor. Biol.* 249 (1), 18–28. 1858
- [73] Lomasko, T., Lumsden, C. J., 2009. One-hit stochastic decline in a 1859
mechanochemical model of cytoskeleton-induced neuron death III: Dif- 1860
fusion pulse death zones. *J. Theor. Biol.* 256 (1), 104–116. 1861
- [74] Macdougall, L., 2015. *Mathematical modelling of retinal metabolism.* 1862
Ph.D. thesis, University of Nottingham. 1863
- [75] Maggelakis, S. A., Savakis, A. E., 1996. A mathematical model of 1864
growth factor induced capillary growth in the retina. *Mathl. Comput.* 1865
Modelling 24 (7), 33–41. 1866
- [76] Maggelakis, S. A., Savakis, A. E., 1999. A mathematical model of reti- 1867
nal neovascularization. *Mathl. Comput. Modelling* 29 (2), 91–97. 1868
- [77] McDougall, S. R., Watson, M. G., Devlin, A. H., Mitchell, C. A., Chap- 1869
lain, M. A. J., 2012. A hybrid discrete-continuum mathematical model 1870
of pattern prediction in the developing retinal vasculature. *Bull. Math.* 1871
Biol. 74, 2272–2314. 1872
- [78] McGuire, B. J., Secomb, T. W., 2001. A theoretical model for oxygen 1873
transport in skeletal muscle under conditions of high oxygen demand. *J.* 1874
Appl. Physiol. 91 (5), 2255–2265. 1875
- [79] Mervin, K., Stone, J., 2002. Regulation by oxygen of photoreceptor 1876
death in the developing and adult C57BL/6J mouse. *Exp. Eye Res.* 1877
75 (6), 715–722. 1878
- [80] Meskauskas, J., Repetto, R., Siggers, J. H., 2012. Shape change of the 1879
vitreous chamber influences retinal detachment and reattachment pro- 1880
cesses: Is mechanical stress during eye rotations a factor? *Invest. Oph-* 1881
thalmol. Vis. Sci. 53 (10), 6271–6281. 1882
- [81] Michaelson, I., 1954. Retinal circulation in man and animals. Thomas. 1883
- [82] Mohand-Saïd, S., Deudon-Combe, A., Hicks, D., Simonutti, M., Forster, 1884
V., Fintz, A. C., Lèveillard, T., Dreyfus, H., Sahel, J. A., 1998. Normal 1885
retina releases a diffusible factor stimulating cone survival in the retinal 1886
degeneration mouse. *Proc. Natl. Acad. Sci.* 95 (14), 8357–8362. 1887
- [83] Mohand-Saïd, S., Hicks, D., Dreyfus, H., Sahel, J. A., 2000. Selective 1888
transplantation of rods delays cone loss in a retinitis pigmentosa model. 1889
Arch. Ophthalmol. 118 (6), 807–811. 1890
- [84] Mohand-Saïd, S., Hicks, D., Simonutti, M., Tran-Minh, D., Deudon- 1891
Combe, A., Dreyfus, H., Silverman, M. S., Ogilvie, J. M., Tenkova, T., 1892
Sahel, J., 1997. Photoreceptor transplants increase host cone survival in 1893
the retinal degeneration (rd) mouse. *Ophthalmic Res.* 29, 290–297. 1894
- [85] Morton, K. W., Mayers, D. F., 2005. Numerical Solution of Partial Dif- 1895

- ferential Equations: An Introduction. Cambridge University Press. 1896
- [86] Murakami, T., Akimoto, M., Ooto, S., Suzuki, T., Ikeda, H., Kawagoe, N., Takahashi, M., Yoshimura, N., 2008. Association between abnormal autofluorescence and photoreceptor disorganization in retinitis pigmentosa. *Am. J. Ophthalmol.* 145 (4), 687–694. 1900
- [87] Murray, J. D., 2002. *Mathematical Biology I: An Introduction*, 3rd Edition. Interdisciplinary Applied Mathematics. Springer. 1902
- [88] Murray, J. D., 2003. *Mathematical Biology II: Spatial Models and Biomedical Applications*, 3rd Edition. Interdisciplinary Applied Mathematics. Springer. 1905
- [89] Pesce, A., Bolognesi, M., Bocedi, A., Ascenzi, P., Dewilde, S., Moens, L., Hankeln, T., Burmester, T., 2002. Neuroglobin and cytoglobin. *fresh blood for the vertebrate globin family.* *EMBO Rep.* 3 (12), 1146–1151. 1908
- [90] Pournaras, C. J., Rungger-Brändle, E., Riva, C. E., Hardarson, S. H., Stefansson, E., 2008. Regulation of retinal blood flow in health and disease. *Prog. Retin. Eye Res.* 27 (3), 284–330. 1911
- [91] Ripps, H., 2002. Cell death in retinitis pigmentosa: Gap junctions and the ‘bystander’ effect. *Exp. Eye Res.* 74 (3), 327–336. 1913
- [92] Roberts, P. A., 2015. *Mathematical models of the retina in health and disease.* D.Phil. thesis, University of Oxford. 1915
- [93] Roberts, P. A., Gaffney, E. A., Luthert, P. J., Foss, A. J. E., Byrne, H. M., 2015. Retinal oxygen distribution and the role of neuroglobin. *J. Math. Biol.* 1918
- [94] Robson, A. G., Saihan, Z., Jenkins, S. A., Fitzke, F. W., Bird, A. C., Webster, A. R., Holder, G. E., 2006. Functional characterisation and serial imaging of abnormal fundus autofluorescence in patients with retinitis pigmentosa and normal visual acuity. *Br. J. Ophthalmol.* 90 (4), 472–479. 1923
- [95] Rossi, T., Boccassini, B., Esposito, L., Clemente, C., Iossa, M., Placentino, L., Bonora, N., 2012. Primary blast injury to the eye and orbit. *Finite element modeling.* *Invest. Ophthalmol. Vis. Sci.* 53 (13), 8057–8066. 1927
- [96] Ruberti, J. W., Roy, A. S., Roberts, C. J., 2011. Corneal biomechanics and biomaterials. *Annu. Rev. Biomed. Eng.* 13 (1), 269–295. 1929
- [97] Salbreux, G., Barthel, L. K., Raymond, P. A., Lubensky, D. K., 2012. Coupling mechanical deformations and planar cell polarity to create regular patterns in the zebrafish retina. *PLoS Comput. Biol.* 8 (8), e1002618. 1933
- [98] Seth, D., 2012. An analytical solution for diffusion and nonlinear uptake of oxygen in the retina. *IJM2C* 2 (3), 181–188. 1935
- [99] Shen, J., Yang, X., Dong, A., Petters, R. M., Peng, Y. W., Wong, F., Campochiaro, P. A., 2005. Oxidative damage is a potential cause of cone cell death in retinitis pigmentosa. *J. Cell Physiol.* 203 (3), 457–464. 1938
- [100] Shintani, K., Shechtman, D. L., Gurwood, A. S., 2009. Review and update: Current treatment trends for patients with retinitis pigmentosa. *Optometry* 80 (7), 384–401. 1941
- [101] Shirinifard, A., Glazier, J. A., Swat, M., Gens, J. S., Family, F., Jiang, Y., Grossniklaus, H. E., 2012. Adhesion failures determine the pattern of choroidal neovascularization in the eye: A computer simulation study. *PLoS Comput. Biol.* 8 (5), e1002440. 1945
- [102] Siggers, J. H., Ethier, C. R., 2012. Fluid mechanics of the eye. *Annu. Rev. Fluid Mech.* 44 (1), 347–372. 1947
- [103] Sneyd, J., Tranchina, D., 1989. Phototransduction in cones: An inverse problem in enzyme kinetics. *Bull. Math. Biol.* 51 (6), 749–784. 1949
- [104] Snodderly, D. M., Weinhaus, R. S., Choi, J. C., 1992. Neural-vascular relationships in central retina of macaque monkeys (*Macaca fascicularis*). *J. Neurosci.* 12 (4), 1169–1193. 1952
- [105] Song, Z., Coca, D., Billings, S., Postma, M., Hardie, R. C., Juusola, M., 2009. Biophysical modeling of a drosophila photoreceptor. In: Leung, C. S., Lee, M., Chan, J. H. (Eds.), *Neural Information Processing*. Vol. 5863 of *Lecture Notes in Computer Science*. Springer Berlin Heidelberg, pp. 57–71. 1957
- [106] Song, Z., Postma, M., Billings, S., Coca, D., Hardie, R., Juusola, M., 2012. Stochastic, adaptive sampling of information by microvilli in fly photoreceptors. *Curr. Biol.* 22 (15), 1371–1380. 1960
- [107] Stefansson, E., 1988. Retinal oxygen tension is higher in light than dark. *Pediatr. Res.* 23, 5–8. 1962
- [108] Stewart, P. S., Jensen, O. E., Foss, A. J. E., 2014. A theoretical model to allow prediction of the CSF pressure from observations of the retinal venous pulse. *Invest. Ophthalmol. Vis. Sci.* 55 (10), 6319–6323. 1963
- [109] Stone, J., Maslim, J., Valter-Kocsi, K., Mervin, K., Bowers, F., Chu, Y., Barnett, N., Provis, J., Lewis, G., Fisher, S. K., Bistid, S., Gargini, C., Cervetto, L., Merin, S., Pe’er, J., 1999. Mechanisms of photoreceptor death and survival in mammalian retina. *Prog. Retin. Eye Res.* 18(6), 689–735. 1964
- [110] Strogatz, S. H., 1994. *Nonlinear Dynamics and Chaos: With Applications to Physics, Biology, Chemistry, and Engineering*. Advanced book program. Westview Press. 1965
- [111] Süli, E., Mayers, D. F., 2003. *An Introduction to Numerical Analysis*. Cambridge University Press. 1966
- [112] Swaroop, A., Kim, D., Forrest, D., 2010. Transcriptional regulation of photoreceptor development and homeostasis in the mammalian retina. *Nat. Rev. Neurosci.* 11, 563–576. 1967
- [113] Tan, P. E. Z., Yu, P. K., Balaratnasingam, C., Cringle, S. J., Morgan, W. H., McAllister, I. L., Yu, D.-Y., 2012. Quantitative confocal imaging of the retinal microvasculature in the human retina. *Invest. Ophthalmol. Vis. Sci.* 53 (9), 5728–5736. 1968
- [114] Till, S. J., Till, J., Milsom, P. K., Rowlands, G., 2003. A new model for laser-induced thermal damage in the retina. *Bull. Math. Biol.* 65 (4), 731–746. 1969
- [115] Tranchina, D., Sneyd, J., Cadenas, I. D., 1991. Light adaptation in turtle cones. testing and analysis of a model for phototransduction. *Biophys. J.* 60 (1), 217–237. 1970
- [116] Travis, G. H., Sutcliffe, J. G., Bok, D., 1991. The retinal degeneration slow (rds) gene product is a photoreceptor disc membrane-associated glycoprotein. *Neuron* 6 (1), 61–70. 1971
- [117] Valter, K., Maslim, J., Bowers, F., Stone, J., 1998. Photoreceptor dystrophy in the RCS rat: roles of oxygen, debris, and bFGF. *Invest. Ophthalmol. Vis. Sci.* 39 (12), 2427–2442. 1972
- [118] Wangsa-Wirawan, N. D., Linsenmeier, R. A., 2003. Retinal oxygen: Fundamental and clinical aspects. *Arch. Ophthalmol.* 121 (4), 547–557. 1973
- [119] Watson, M. G., McDougall, S. R., Chaplain, M. A. J., Devlin, A. H., Mitchell, C. A., 2012. Dynamics of angiogenesis during murine retinal development: a coupled in vivo and in silico study. *J. R. Soc. Interface* 9 (74), 2351–2364. 1974
- [120] Yang, Y., Mohand-Said, S., Danan, A., Simonutti, M., Fontaine, V., Clerin, E., Picaud, S., Leveillard, T., Sahel, J. A., 2009. Functional cone rescue by RdCVF protein in a dominant model of retinitis pigmentosa. *Mol. Ther.* 17 (5), 787–795. 1975
- [121] Young, R. W., 1967. The renewal of photoreceptor cell outer segments. *J. Cell Biol.* 33 (1), 61–72. 1976
- [122] Young, R. W., 1971. The renewal of rod and cone outer segments in the rhesus monkey. *J. Cell Biol.* 49, 303–318. 1977
- [123] Young, R. W., 1978. The daily rhythm of shedding and degradation of rod and cone outer segment membranes in the chick retina. *Invest. Ophthalmol. Vis. Sci.* 17 (2), 105–116. 1978
- [124] Young, R. W., Bok, D., 1969. Participation of the retinal pigment epithelium in the rod outer segment renewal process. *J. Cell Biol.* 42, 392–403. 1979
- [125] Yu, D. Y., Cringle, S., Valter, K., Walsh, N., Lee, D., Stone, J., 2004. Photoreceptor death, trophic factor expression, retinal oxygen status, and photoreceptor function in the P23H rat. *Invest. Ophthalmol. Vis. Sci.* 45 (6), 2013–2019. 1980
- [126] Yu, D. Y., Cringle, S. J., 2001. Oxygen distribution and consumption within the retina in vascularised and avascular retinas and in animal models of retinal disease. *Prog. Retin. Eye Res.* 20 (2), 175–208. 1981
- [127] Yu, D. Y., Cringle, S. J., 2002. Outer retinal anoxia during dark adaptation is not a general property of mammalian retinas. *Comp. Biochem. Physiol.* 132 (1), 47–52. 1982
- [128] Yu, D. Y., Cringle, S. J., 2005. Retinal degeneration and local oxygen metabolism. *Exp. Eye Res.* 80 (6), 745–751. 1983
- [129] Yu, D. Y., Cringle, S. J., Balaratnasingam, C., Morgan, W. H., Yu, P. K., Su, E. N., 2013. Retinal ganglion cells: Energetics, compartmentation, axonal transport, cytoskeletons and vulnerability. *Prog. Retin. Eye Res.* 36, 217–246. 1984
- [130] Zhu, C. L., Ji, Y., Lee, E.-J., Grzywacz, N. M., 2013. Spatiotemporal pattern of rod degeneration in the S334ter-line-3 rat model of retinitis pigmentosa. *Cell Tissue Res.* 351 (1), 29–40. 1985
- [131] Zouache, M., Eames, I., Luthert, P., 2015. Blood flow in the choriocapillaris. *J. Fluid Mech.* 774, 37–66. 1986